



HAL
open science

Probing the Electronic Properties and Interaction Landscapes in a Series of N -(Chlorophenyl)pyridinecarboxamides

John F Gallagher, Niall Hehir, Pavle Mocilac, Chloé Violin, Brendan F O'connor, Emmanuel Aubert, Enrique Espinosa, Benoît Guillot, Christian Jelsch

► **To cite this version:**

John F Gallagher, Niall Hehir, Pavle Mocilac, Chloé Violin, Brendan F O'connor, et al.. Probing the Electronic Properties and Interaction Landscapes in a Series of N -(Chlorophenyl)pyridinecarboxamides. *Crystal Growth & Design*, 2022, 22 (5), pp.3343-3358. 10.1021/acs.cgd.2c00153 . hal-03811332

HAL Id: hal-03811332

<https://hal.science/hal-03811332>

Submitted on 11 Oct 2022

HAL is a multi-disciplinary open access archive for the deposit and dissemination of scientific research documents, whether they are published or not. The documents may come from teaching and research institutions in France or abroad, or from public or private research centers.

L'archive ouverte pluridisciplinaire **HAL**, est destinée au dépôt et à la diffusion de documents scientifiques de niveau recherche, publiés ou non, émanant des établissements d'enseignement et de recherche français ou étrangers, des laboratoires publics ou privés.

PROBING THE ELECTRONIC PROPERTIES AND INTERACTION LANDSCAPES IN A SERIES OF *N*-(CHLOROPHENYL)PYRIDINECARBOXAMIDES

John F. Gallagher,* Niall Hehir, Pavle Mocilac, Chloé Violin, Brendan F. O'Connor[#]

School of Chemical Sciences, Dublin City University, Dublin 9, Ireland

School of Biotechnology, Dublin City University, Dublin 9, Ireland.[#]

and

Emmanuel Aubert, Enrique Espinosa, Benoît Guillot, Christian Jelsch

CRM², CNRS UMR 7036, Faculté des Sciences et Technologies, Université de Lorraine,

BP 70239, Boulevard des Aiguillettes, 54506 Vandoeuvre-lès-Nancy, France

ABSTRACT

A 3 × 3 isomer grid of nine *N*-(chlorophenyl)pyridinecarboxamides (**NxxCl**) is reported with physicochemical studies and single crystal structures (**Nx** = pyridinoyl moiety; **xCl** = aminochlorobenzene ring; **x** = *para*-/*meta*-/*ortho*-). Reaction of the substituted *p*-/*m*-/*o*-pyridinecarbonyl chlorides (**Nx**) with *p*-/*m*-/*o*-aminochlorobenzenes (**xCl**) yields the nine compound **NxxCl** series. Several of the nine **NxxCl** crystal structures display structural similarities with their halogenated **NxxX** and methylated **NxxM** relatives (**x** = *p*-/*m*-/*o*-substitutions; **X** = F, Br; **M** = methyl). Indeed, five of the nine **NxxCl** crystal structures are isomorphous with their **NxxBr** analogues as the **NpmCl/Br**, **NpoCl/Br**, **NmoCl/NmoBr**, **NopCl/Br** and **NooCl/Br** pairs. In the **NxxCl** grid, the favoured hydrogen bonding mode is aggregation by N-H...N_{pyridine} interactions, though amide...amide intermolecular interactions are noted in **NpoCl** and **NmoCl**. For the **NoxCl** triad, intramolecular N-H...N_{pyridine} interactions influence molecular planarity, whereas **NppCl•H₂O** (as a monohydrate) exhibits O-H...O, N-H...O1W and O1W-H...N interactions as the primary hydrogen bonding. Analysis of chlorine-containing compounds on the CSD is noted for comparisons. The interaction environments are probed using Hirshfeld surface analysis and contact enrichment studies. The melting temperatures T_m depend on both the lattice energy and on molecular symmetry (Carnelley's rule). The melting points can be well predicted from a linear regression of the two variables. The relationships of the T_m values with the total energy, the electrostatic component and the strongest hydrogen bond components were analyzed.

KEYWORDS Carboxamide; Chlorine; Conformational analysis; Contact Enrichments; Crystal structure; Halogen; Melting Points; Structural systematics.

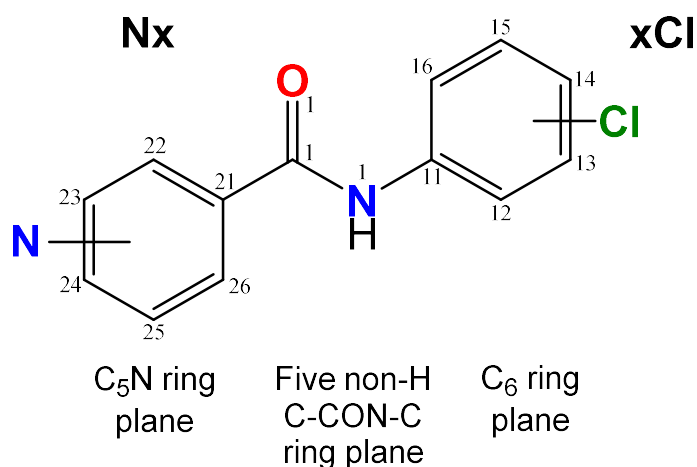
Corresponding author:* Dr. John F. Gallagher, School of Chemical Sciences, Dublin City University, Dublin 9, Ireland e-mail address: john.gallagher@dcu.ie

Introduction:

Organohalogens (as a class of organic chemicals) have seen a dramatic increase in research activity over the past three decades in a range of scientific fields such as atmospheric chemistry, pharmaceuticals and agrochemicals.¹⁻³ These research studies include both basic and applied research, together with industrial applications. On-going structural chemistry research on organohalogens include investigations on halogen bonding and intermolecular interactions; these studies have led to considerable developments and insights into our understanding of bonding and aggregation modes.⁴⁻⁵ Extensive structural studies have been undertaken on series of organohalogens. Examples include the investigation of fluorine in benzamides⁶ and the potential uses of bromine and iodine in agrochemicals.⁷

Organochlorines have attracted considerable interest in pharmaceuticals⁸ and especially in agrochemicals (herbicides and pesticides) with uses as antihelminthic drugs such as Niclosamide (an orally bioavailable chlorinated salicylanilide).^{8b} Some of these have raised public concern mainly due to their disposal, waste treatment and environmental problems.^{1,3,9} In tandem in drug development, there has been a surge in the study and use of halogens in new drugs and especially fluorine and chlorine in pharmaceuticals.^{6,8}

The role and importance of the Cambridge Structural Database (CSD) as a tool for understanding structural systematics has been noted.¹⁰ As such the development of structural systematics in pharmaceutical sciences is critical as one seeks to establish correlations in physicochemical relationships between series of molecules. In analysing the electronic properties of series of compounds (such as $n \times m$ carboxamide isomer grids), the ability to observe trends in fundamental properties is essential. As advances in this area continue to be made, it is essential that our ability to assess tens, hundreds or thousands of related structures is made easier. A key is to reduce the number of parameters and elucidate genuine relationships and correlations in order to aid in the development of new drugs.^{2,8,10}



Scheme 1:

The **NxxCl** series of molecules with **Nx** representing the C₅H₄NC=O (pyridinoyl) and **xCl** the -HNC₆H₄Cl (aminochlorobenzene) moieties (**x** = *para*-/*meta*-/*ortho*-substitutions).

The numbering scheme as used in the inter-planar calculations (non-H atoms only) and **Figures 1-6**, is shown.

We have previously reported several series of benzamides and carbamates including the mono-substituted, methyl-, fluoro- and chlorobenzamides and the related methyl and methoxycarbamates.¹¹⁻¹² In expanding the isomer grid series, the increased numbers of compounds for analysis and for comparisons can be appreciated with what is already available for study on the CSD.¹⁰ In analysing electronic structure, one can ascertain the effects at the intramolecular and intermolecular level and derive trends, correlations in isoelectronic series of molecules such as the nine-member **NxxCl** series (**Scheme 1**). The *N*-(chlorophenyl)pyridinecarboxamide series is described herein and used for comparisons with other related isomer grids.¹¹⁻¹² The **NxxCl** compounds are readily synthesised from the three *p*-/*m*-/*o*-pyridinoyl chlorides and three *p*-/*m*-/*o*-aminochlorobenzene isomers using standard synthetic procedures. They are chemical analogues of the related *N*-(fluorophenyl)pyridinecarboxamide (**NxxF**) isomer grid.^{11a} The single crystal structures (**Figures 1-6**), conformational analyses and physicochemical properties of **NxxCl** are described (**Figures 7-13**). Together, these are analysed to highlight correlations with crystal properties and molecular charge densities and also to make notable comparisons with related series of molecules.¹¹

Experimental:

Materials, Methods and Equipment

All chemicals, materials, vendors, spectroscopic and crystallographic methods together with computational programs and equipment are as reported previously.¹¹⁻¹² Chemicals and silica (Davisil) were used as purchased from Sigma Aldrich; TLC alumina, silica plates from Fluka. Melting points were measured using a Stuart Scientific SMP40 automated melting point apparatus. IR spectroscopy was recorded using a Perkin Elmer Spectrum GX FTIR spectrometer by the attenuated total reflection (ATR) method: spectral bands are quoted in cm^{-1} . NMR spectroscopy was performed on a Bruker BioSpin UltraShield NMR spectrometer (293±1 K), at 400 or 600 MHz for ^1H and 100.62 MHz for the ^{13}C resonance. The ^1H spectra were recorded in CDCl_3 and $\text{DMSO}-d_6$ with the ^{13}C spectra analyzed in CDCl_3 . The NMR chemical shift values (δ) are in ppm, referenced to TMS and coupling constants (J) are quoted in Hz.

Single crystal X-ray data collections for the nine **NxxCl** crystal structures (**Scheme 1**) together with data reduction, structure solution and refinements,^{13a-c} are as described for the previously reported 3×3 isomer grids¹¹⁻¹² and are fully detailed in the ESI (Tables S1). Selected crystallographic and structural information are analysed and compiled with pertinent structural details provided in the main paper in **Tables 1, 2**.¹³ Molecular structures and hydrogen bonding diagrams (**Figures 1-6**) are depicted with displacement ellipsoids drawn at the 30% probability level.^{13d,e} The computational calculations¹⁴ were performed as described previously.¹¹⁻¹² Optimisations and conformational analyses in *gas phase* were performed using the DFT method [B3LYP/6-311++G(d,p)].^{14b,c} All calculations were performed using Gaussian09^{14a} for Linux/Unix operating on a SGI Altix ICE 8200EX high

performance computing system at the ICHEC (Galway, Ireland). The *gas phase* data are presented in a diagram as a 3×3 grid to highlight trends in the position of the substituent and displayed from the *pp* to *oo* (**Figure 12**; in ESI Section II as enlarged diagrams).

Table 1: Selected crystallographic data for **NxxCl** (full details available; Table S1 in ESI)

Structure	Crystal system; Space group	Z'	Volume (Å ³)	R, wR ₂ R-factors, GoF
NppCl•H₂O	Orthorhombic; <i>Pbca</i>	1	2344.89(8)	0.042, 0.108, 1.03
NpmCl	Monoclinic; <i>P2₁/n</i>	1	1090.45(4)	0.035, 0.102, 1.07
NpoCl	Monoclinic; <i>Cc</i>	1	1108.06(11)	0.026, 0.067, 1.10
NmpCl	Monoclinic; <i>P2₁</i>	1	531.27(3)	0.043, 0.114, 1.03
NmmCl	Monoclinic; <i>P2₁/n</i>	1	1068.45(4)	0.038, 0.115, 1.11
NmoCl	Monoclinic; <i>P2₁/c</i>	1	1078.89(9)	0.066, 0.149, 1.08
NopCl	Triclinic; <i>P-1</i>	1	543.73(3)	0.038, 0.105, 1.05
NomCl	Triclinic; <i>P-1</i>	1	532.00(5)	0.038, 0.124, 1.08
NooCl	Orthorhombic; <i>Pbca</i>	1	2226.2(11)	0.051, 0.120, 0.89

Footnote: R-factor definitions as $R[F^2 > 2\sigma(F^2)]$, $wR(F^2)$.^{13a}

The average **NxxCl** molecular volume (*i.e.* cell volume (Å³)/Z) is 273 Å³ and discounting the **NppCl** monohydrate. The largest molecular volumes are **NooCl** (278 Å³) and **NpoCl** (277 Å³). The smallest volumes are for the **NmpCl** and **NomCl** structures (both 266 Å³). The calculation for **NppCl•H₂O** is at ~255 Å³ per **NppCl** and taking into account the volume of the tightly bound monohydrate molecule (as ~38 Å³).^{13d}

Table 2: Salient **NxxCl** structural features (inter-planar angles, distances, interactions in Å, °).

Structure	C ₆ /C ₅ N (°)	C ₆ /amide (°)	C ₅ N/amide (°)	N...N/O [#] (Å)	Primary H bonds
NppCl•H₂O	47.68(5)	7.58(7)	40.43(5)	2.831(2)* 2.838(3)* 2.903(2)*	Hydrate packing (2 × N...O/O...O)
NpmCl	1.52(9)	17.96(6)	18.23(7)	3.1373(17)	Amide...Pyridine
NpoCl	83.24(7)	69.59(8)	27.43(11)	2.797(2) [#]	Amide...Amide
NmpCl	7.65(14)	32.11(10)	32.02(9)	3.079(3)	Amide...Pyridine
NmmCl	56.53(4)	30.44(4)	27.03(5)	3.0842(13)	Amide...Pyridine
NmoCl	16.30(17)	38.87(17)	25.54(15)	2.884(3) [#]	Amide...Amide
NopCl	2.86(7)	1.26(7)	1.75(7)	<u>2.6631(16)</u>	Intra as (N-H...N)
NomCl	1.07(6)	7.86(5)	6.91(5)	<u>2.6536(13)</u>	Intra as (N-H...N)
NooCl	8.6(2)	9.7(2)	1.2(2)	<u>2.624(4)</u>	Intra as (N-H...N)

Footnote: C₆ is the (C11,...,C16) benzene plane; C₅N is the (C21,...,C26) pyridine ring plane and the amide is represented by the five atom C21-C1(=O1)N1-C11 plane (**Scheme 1**) and with reference to **Figures 1-6**.

* **NppCl** monohydrate structure with N1...O1W, O1W...O1 and O1W...N1 hydrogen bonding.

[#] represents N...O (amide...amide) with the intramolecular N...N interactions underlined.

Methods¹⁵

The electrostatic energy E_{elec} was computed from the charge density models transferred from the ELMAM2 database of multipolar atoms^{15a} using the MoProSuite software.^{15b} The structures as obtained from SHELX refinement were modified by elongation of the N-H and C-H bonds to standard distances retrieved from neutron diffraction studies.^{15c} The molecules were rendered electrically neutral after charge density transfer by applying a uniform valence population shift to all atoms. The electrostatic energy between interacting molecules was obtained by summation over pairs of multipolar charged atoms belonging to each entity. The lattice electrostatic energy was computed with the VMoPro module in real space. The energy was summed over successive parallelepiped shells surrounding the unit cell. The summations were carried over the $[-9\mathbf{a},9\mathbf{a}] \times [-9\mathbf{b},9\mathbf{b}] \times [-9\mathbf{c},9\mathbf{c}]$ space around the molecule containing 19^3 unit cells where convergence is largely achieved.

The total energy was computed with the CrystalExplorer19 software^{15d} between the asymmetric unit and a cluster of surrounding molecules within a distance of 3.80 Å. The energy components calculated within this procedure are electrostatic, polarization, dispersion, and exchange-repulsion and finally the total interaction energy. These energy calculations were performed at the B3LYP/6-31G** level of theory.^{14b,c} The structures used were the same as for the electrostatic energy calculation on the multipolar model. Diagrams are included in the main paper text as **Figures 8-11** and in the supplementary information (ESI Section IV pgs 56-68) as **Figures S01-S06**.

Results and Discussion

NxxCl crystal structures:

The nine *N*-(chlorophenyl)pyridinecarboxamide crystal structures (**NxxCl**) are grouped in triads for structural comparisons with pertinent structural data presented in **Tables 1, 2**. Comparisons are made with the **Clxx** series^{11g} (as their amide bridge reversed isomers) together with the related **NxxF**,^{11a} (methyl) **NxxM**,^{11b} and **NxxBr** analogues.^{11e}

The NpxCl triad:

NppCl crystallises as a monohydrate with the amide N-H donor, O=C and N_{pyridine} acceptor groups engaged in hydrogen bonding interactions with the water molecule O1W. In the crystal structure, two **NppCl•H₂O** aggregate through (_{amide}N1-H1...O1W-H2W...N24_{pyridine}) hydrogen bonds and form *R*⁴₄(18) hydrogen bonded rings about inversion centres (**Figure 1**). The (**NppCl•H₂O**)₂ units are linked by 2 × (O1W-H1W...O1=C1) and 2 × (C1=O1...H1W-O1W) hydrogen bonds per aggregate. These four strong intermolecular interactions form a 2D sheet that is effectively ~21 Å wide. Overall, 2D sheets interlock into a 3D structure by using 2 × (C13-H13...O1=C1) and 2 × (C1=O1...H13-C13) weak H-bonds per aggregate. This hydrate aggregation is similar to related benzamide hydrates with all strong hydrogen bonding donors and acceptors used.¹⁶ The closest contacts with the *para*-chlorine Cl14 atom involve three H atoms (H23, H25, H26) on symmetry related molecules, but with all of the H...Cl14 distances larger than 3.0 Å).

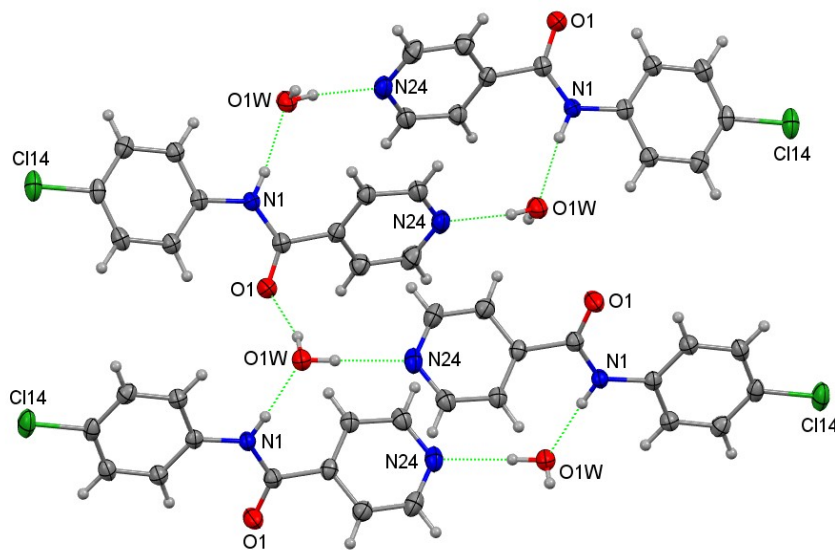


Figure 1: A view of [**NppCl•H₂O**]₂ linked by an O1W-H2W...O1 interaction.

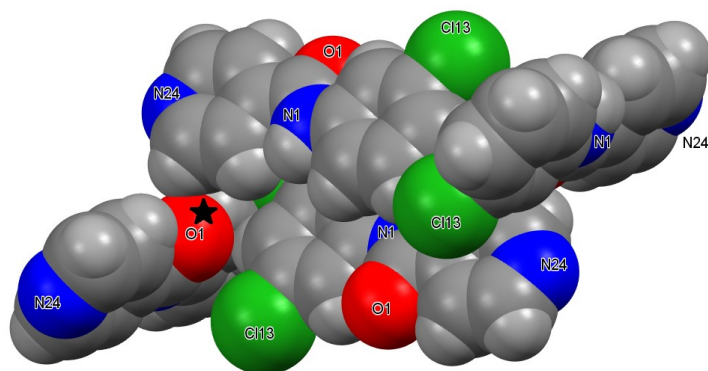


Figure 2: A view of the C-H...O1=C1 interactions in **NpmCl**.

NpmCl and **NpoCl** structures: *isomorphous behaviour*¹⁷

NpmCl is isomorphous with **NpmM**^{11b} and **NpmBr**^{11e} in the monoclinic space group $P2_1/n$, but is not isomorphous with **NpmF**^{11a} (see below). The hydrogen bonded N-H...N chains in **NpmCl** contrast with conventional N-H...O=C (amide...amide) interactions in **NpoCl**. Furthermore, two C-H...O=C contacts are noted in **NpmCl** in the absence of N-H...O=C interactions (**Figure 2**). The amide...pyridine N-H...N_{pyr} hydrogen bonded chains are augmented by two weaker C-H...N_{pyr} interactions. There are up to six Cl...H-C close contacts at $d_{\text{HCl}} < 3.6$ Å with symmetry related molecules, though the shortest distance, H15...Cl13, is larger than 3.2 Å. In **NpoCl**, amide...amide hydrogen bonding as 1D chains along the *c*-axis direction is the primary interaction mode (**Figure 3**). Chains are weakly linked by C-H...N_{pyridine} contacts. **NpoCl** is isomorphous with both **NpoM**^{11b} and **NpoBr**^{11e} in space group *Cc*, but differs slightly from the **NpoF** and **NpmF** structures where N-H...N interactions dominate. However, both **NpxF** structures also crystallise in space group *Cc* and the series of structures can be considered as being on the continuum of isomorphous behaviour.^{10,11c} In **NpoCl** the closest contacts between the chlorine Cl12 and H atoms involve H13 on a symmetry related molecule (though with H13...Cl12 > 3.1 Å). Therefore, in summary, both **NpmCl** and **NpoCl** exhibit isomorphous behaviour with their methylated (**M**) and brominated (**Br**)^{11e} congeners but not with their fluorinated analogues (**F**).

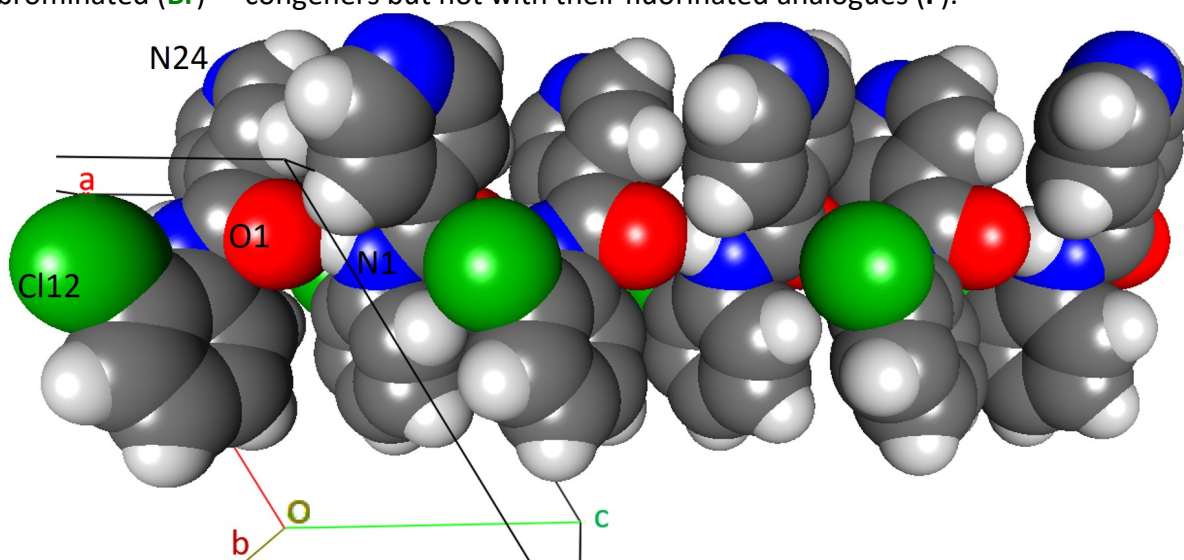


Figure 3: Crystallographic autostereogram of the 1D amide...amide chains along the *c*-axis in **NpoCl** (atoms drawn as van der Waals spheres).

The NmxCl triad

The **NmxCl** triad structures are not isomorphous with any of their **NmxF**,^{11a} **NmxM**,^{11b} congeners although there is an isostructural relationship between **NmmCl** and **NmmF**. **NmpCl** aggregates by *zig-zag* amideN-H...N_{pyridine} chains of interactions along the *b*-axis direction in the monoclinic space group $P2_1$ and forms a 2D herringbone structure ~16.5 Å wide (**Figure 4**). Chains are linked by C-H...O=C interactions and forming a rumped sheet. Short C22-H22...C22^{5a,c} interactions form relays of contacts in tandem with amideN-H...N_{pyridine}. The Cl14 atoms are not involved in any strong hydrogen or halogen bonding and are positioned in the lattice while involved in multiple aromatic H atom contacts. The closest being the Cl14 and H25 atoms on symmetry related molecules with H25...Cl14 at ~3.0 Å).

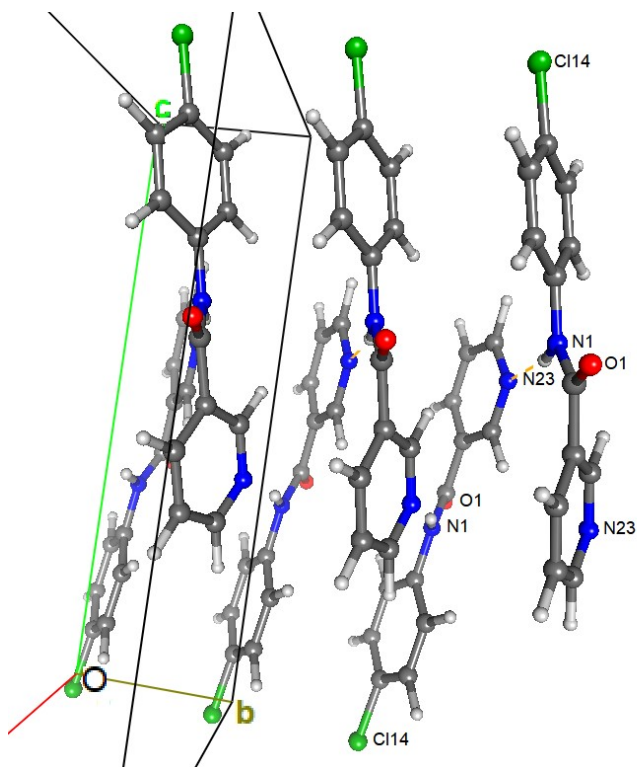


Figure 4:
Crystallographic autostereogram of the amideN-H...N_{pyridine} zig-zag chains in **NmpCl**.

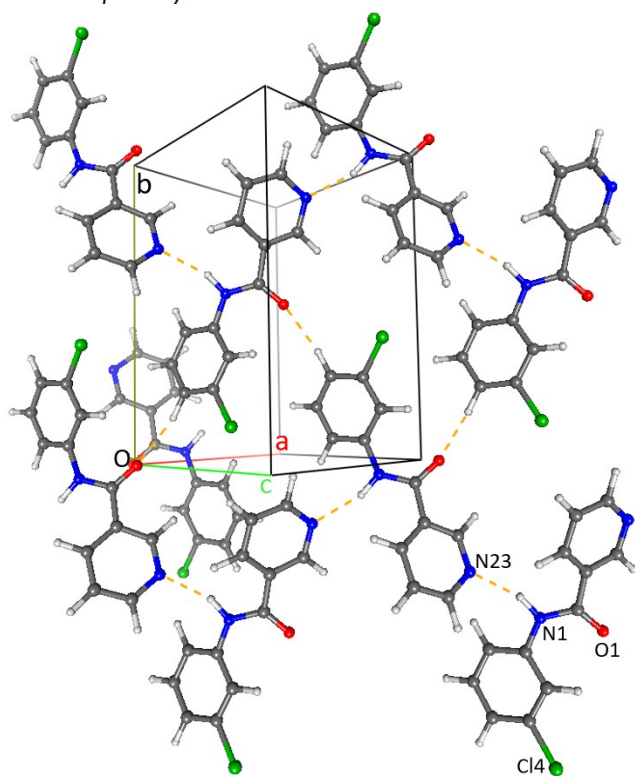


Figure 5:
Crystallographic autostereogram showing the 1D zig-zag N-H...N chains as linked by C-H...O interactions in **NmmCl**.

NmmCl with 1D zig-zag N-H...N chains is (at least) isostructural with **NmmF** in space group $P2_1/n$. Aggregation is assisted by alignment of 1D chains *via* C14-H14...O1 interactions and formation of 2D sheets (**Figure 5**). In doing so, series of tetrameric units are generated in the **NmmCl** crystal structure and with C-H... π (arene) interactions generate ruffled sheets. In contrast, **NmoCl** is isomorphous with **NmoBr**^{18a} (**TICDOZ01**)¹⁰ with N-H...O=C intermolecular interactions along the *b*-axis direction and short intramolecular interactions between the

ortho-Cl12 and the N-H group. In addition, there are Cl12...C14 contacts between the *ortho*-Cl12 and symmetry related chlorinated aromatic rings.

The NoxCl triad: relatively planar molecules with aromatic stacking

All three **NoxCl** have their benzene and pyridine rings aligned close to co-planarity (**Table 2**); this is largely influenced by two intramolecular N-H...N and C-H...O interactions. Both **NopCl** (reported previously as **GEPQIC**)^{18b} and **NooCl** are isomorphous with the **NopBr** and **NooBr** congener structures,^{11e} respectively.¹⁷ The **NopCl** crystal structure with an intramolecular N1-H1...N22_{pyridine} contact has aromatic stacking and long distance C-H...O/Cl interactions ($d_{\text{HCl}}=2.88 \text{ \AA}$) resulting in 2D sheet formation. Likewise, **NomCl** has two intramolecular H-bonds per molecule: the short N1-H1...N22 and a weaker C-H...O contact. Consequently, there are no strong intermolecular hydrogen bonds (but only two C-H...O and one C-H...Cl ($d_{\text{HCl}}\sim 2.90 \text{ \AA}$) weak H-bonds; the closest C...C aromatic stacking distance is $3.4873(17) \text{ \AA}$.^{5f} **NooCl**, isomorphous with **NooBr**,^{11e} is relatively planar due to the intramolecular Cl22...H1(N1)...N22 bifurcated hydrogen bonding arrangement (**Figure 6**) and is similar in structure to **NooF**,^{11a} **NooM**^{11b} and **Cl-NooM** (a side-product from the **NooM** synthesis).^{11b} The intermolecular interactions are typically weak and comprise C-H...O and C-H... π (arene) contacts (with C...C aromatic stacking distances $\geq 3.60 \text{ \AA}$). Overall, the relatively planar **NoxCl** triad compares well with the **NoxM**, **NoxF** and **Cl-NoxM** series, and in each of these series, it is usually the *para*-derivative that has its arene rings twisted most from co-planarity.^{11a,b}

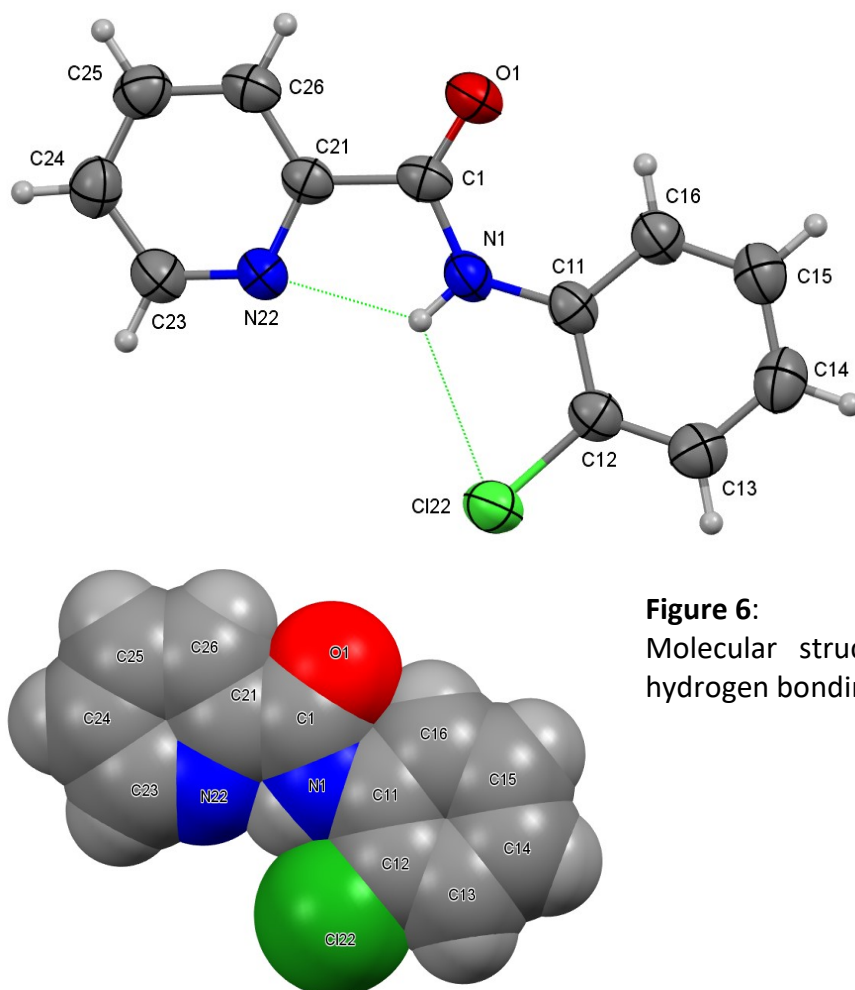


Figure 6: Molecular structure and intramolecular hydrogen bonding in **NooCl**.

Isomorphous relationships: summary and analysis of NxxCl and NxxBr^{11e,17}

Isomorphous relationships between structures in the 3×3 isomer grids show overlap between five NxxCl isomers and their NxxBr analogues (as the NpmCl/Br, NpoCl/Br, NmoCl/Br,^{18a} NopCl^{18b}/Br, NooCl/Br pairs). This correlates well with what has been noted with five of the Clxx/Brxx amide-bridge reversed analogues (see Table 3).^{11e,g} Furthermore, for the 'pm' or 'po' sets of crystal structures, the methylated analogues NpmM and NpoM are isomorphous with the Cl/Br pairs and further extend the structural series overlap.

Table 3: Isomorphous relationships between NxxCl^{this work} and NxxBr^{11e,18a}: comparisons with the amide-bridge reversed Clxx^{11g} and Brxx.^{11e,17}

NxxCl and NxxBr isomer grids			Clxx and Brxx isomer grids		
NxxCl	Space group	NxxBr ^{11e}	Clxx ^{11g}	Space group	Brxx ^{11e}
NppCl•H ₂ O	Pbca ⇔ P2 ₁	NppBr	Clpp	<i>P2₁/c</i>	Brpp
NpmCl	<i>P2₁/n</i>	NpmBr	Clmp (Z'=4)	P-1 ⇔ P-1	Brmp (Z'=2)
NpoCl	<i>Cc</i>	NpoBr	Clpo	<i>Pbca</i>	Broo
NmpCl	P2 ₁ ⇔ C2/c	NmpBr	Clpm	P-1 ⇔ C2/c	Brpm
NmmCl	P2 ₁ /n ⇔ P-1	NmmBr	Clmm•H ₂ O	<i>P2₁/c</i>	Brmm•H ₂ O
NmoCl	<i>P2₁/c - P2₁/a</i>	NmoBr ^{18a}	Clom	<i>C2/c</i>	Brom
NopCl ^{18b}	<i>P-1</i>	NopBr	Clpo	C2/c ⇔ P-1	Brpo
NomCl	P-1 ⇔ C2/c	NomBr	Clmo	P-1 ⇔ P2 ₁ /c	Brmo
NooCl	<i>Pbca</i>	NooBr	Cloo	<i>C2/c</i>	Broo

Footnote: Isomorphous pairs are highlighted in bold with their common space group in *italics*.

The ⇔ symbol is for crystal structures that are not isomorphous; for Clmp and Brmp, Z' is noted.

Clxx and Brxx have to be understood as ClxxN and BrxxN, but are noted this way in articles ^{11g} and ^{11e,17}.

In Table 3, ten of the 18 structural pairs from the Clxx/Brxx and NxxCl/NxxBr isomer grids are isomorphous.¹⁷ These results support an extensive Cambridge Structural Database (CSD) study by Mukherjee and Desiraju^{4d,10} where they noted a significant degree of similarity between pairs of structures presenting C-X bonds (X = Cl or Br).^{4d} Such pairs are observed to adopt the same space group, number of molecules in the unit cell and reduced unit cell parameters (within 1 Å). Using this, our study is to compare the Clxx^{11g} grid with the NxxCl series and make structural comparisons with the Brxx and NxxBr analogues.^{11e}

The extent of isomorphous behaviour between pairs of structures in the Cl/Br series is much greater than that noted for the Me/F or F/Cl analogous pairs (NmmF and NmmCl are isostructural in P2₁/n).¹¹ Moreover, there are examples where three structures exhibit isomorphous behaviour e.g. the NpmM, NpmCl, NpmBr triad is isomorphous in the monoclinic space group P2₁/n. Furthermore, NpoM, NpoCl, NpoBr are isomorphous in space group Cc and are aggregating by amide...amide interactions.¹¹ However, NpoF (and NpmF) differ in structure using amide...pyridine interactions, though also crystallising in space group Cc.^{11c} Of note are the isostructural Clmp (Z'=4) and Brmp (Z'=2) with two sets of similar unit cell axes in Clmp (a, b) and Brmp (b, c) and with the third axis (a) halved in Brmp (ESI: Table S4b). This represents the extent of overlap within these classes of functionalised benzamides.¹¹ There is an extensive 'pp' series with several closely related crystal structures.^{11c,g} There are, however, no pairs of isomorphous NxxCl/Clxx structures involving amide-bridge swapped isomers e.g. NomCl/Clmo, as noted in the NmmM and Mmm crystal

structures.^{11b,d;17,19} Ojala and co-workers have commented on bridge-flipped isomers in extensive series of benzylideneanilines and phenylhydrazones.¹⁹ In our series, the amide group N–H dominates as a pivot in the crystal structure and together with the N_{pyridine} and halogen X reduces the possibility of bridge-flipping or amide-bridge swapping.¹¹

The general trend for **Cl/Br** pairs of isomorphous structures is interesting,^{4d,10} and, in some cases, a methyl analogue (**NxxM**)^{11b} is isomorphous with the **Cl/Br** pairs (**NmoCl/NmoBr**^{18a}; **NmoM/NmoBr**^{18c} with **NmoBr** polymorphs^{18a,c}). However, it is also notable that the fluorinated **Fxx**^{6b,11c}/**NxxF**^{11a} do not tend to form isomorphous relationships with **Me**, **F** or **Cl** to the same extent as the **Clxx**^{11g}/**Brxx**^{11e,17} and **NxxCl**^{herein}/**NxxBr**^{11e} groups of structures.

Structural aspects of organic chlorine:

Fluorine has been extensively analysed in terms of intermolecular interactions and contacts by using the CSD and other analytical methods.^{6,10,20} Chlorine contrasts with fluorine as it is often present as chlorinated solvents such as CH₂Cl₂ or CHCl₃ solvates in crystal structures.

Analysis of C–H...Cl intermolecular interactions in molecular crystals as a function of the hybridization of the donor atom and acceptor atoms shows the C_(sp2)–H...Cl–C_(sp2) to be prevalent. Furthermore, upon cone correction, this type of C_(sp2)–H...Cl intermolecular interaction exhibits a clear preference for angularity of ~120° with the area approaching linearity also dominant. Analysis of N–H...Cl–C and O–H...Cl–C intermolecular interactions shows that they are less common than C–H...Cl–C interactions based on a statistical analysis as noted by the decrease in observed 'hits'.¹⁰ This was also noted in the analysis of several families of halogenated organic molecules by the contacts enrichment ratio^{20b} which confirmed that organic halogen atoms prefer to interact with the lowly charged H_C hydrogen atoms (bound to a carbon atom) rather than with H_O atoms (bound to O). On the other hand, O and N atoms, which are stronger H-bond acceptors tend to form H-bonds with the more polar H_N and H_O hydrogen atoms.

The methodology described could be extended to investigate intermolecular interactions involving various other halogenated organic molecules containing bromine or iodine atoms. This is expected to provide a deeper understanding into the nature of such contacts and into the characteristics of interactions as a whole. Such analyses should be viewed in tandem with the structural similarity approach used by Mukherjee and Desiraju in their CSD study.^{4d,10}

Infra-red analysis:

The ATR-IR spectra of all **NxxCl** derivatives are clear and can be correlated with their solid-state structures. For example, in comparison of the **NxpCl** spectra (**Figure 7**; ESI pg 55, ATR-IR diagram), three distinct spectra are observed as would be expected from calculated results. Indeed, **NppCl•H₂O** forms N–H...O–H...O=C and O–H...N_{pyridine} intermolecular hydrogen bonds involving **NppCl** and the water molecule (**Scheme 2**). Its spectrum contains a band at 3470 cm⁻¹ indicating water of crystallisation (in the crystal structure as **NppCl•H₂O**).¹⁶

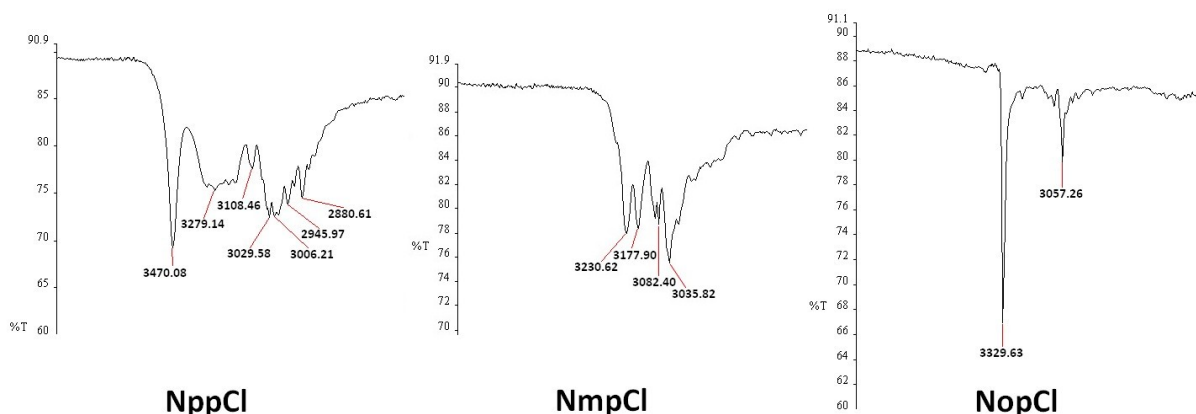
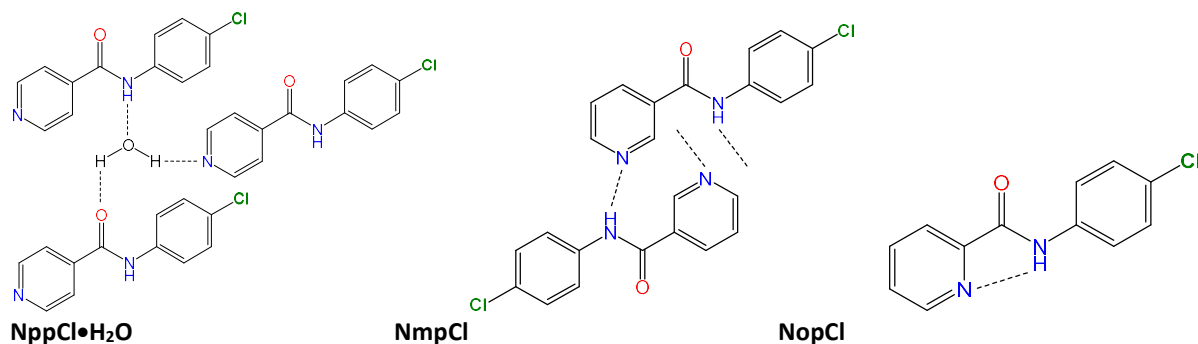


Figure 7: ATR-IR spectra of the **NxpCl** triad.

As expected, the **NppCl** molecule has two potentially strong acceptor groups, N_{pyridine} and amide $C=O$, with one donor $N-H$ group. It interacts with water having two potential $O-H$ donors and either one or two acceptors as the O atom electron lone pairs. This effectively balances the total number of donors/acceptors in the crystal structure of **NppCl**• H_2O .



Scheme 2: Intermolecular hydrogen bonding in **NppCl**• H_2O , **NmpCl** and intramolecular hydrogen bonding in **NopCl**.

Two distinct IR bands at 3231 and 3178 cm^{-1} in the **NmpCl** spectrum reveal an intermolecular hydrogen bond. This is as expected from the crystal structure results for the catemeric $N-H...N_{\text{pyridine}}$ chains arising in **NmpCl** (**Figure 4**). This is further highlighted for the **NoxCl** triad due to the presence of an intramolecular $N-H...N_{\text{pyridine}}$ interaction. In the **NopCl** spectrum, the very sharp strong band at 3330 cm^{-1} indicates there is no strong intermolecular hydrogen bonding. For the **NoxCl** triad, the spectrum is indicative of an intramolecular hydrogen bond (**Scheme 2**) as noted in the **NoxF**^{11a} and **NoxM**^{11b} triads. Indeed, as shown in the ESI (ATR-IR Figure), there is a high degree of correlation between the interactions in the nine **NxxCl** crystal structures and their respective ATR-IR spectra. In structures with similar primary hydrogen bonding *e.g.* **NoxCl**, the ATR-IR spectra show similar features.

Melting point analysis²¹

Comparisons between the **Clxx** and **NxxCl** melting points are essential and especially where there are structural relationships between the two series of isomers (**Table 4**). In previous work on related systems (**NxxF**, **NxxM**, **Fxx**, **Mxx**)^{11a-d}, it has been shown that there is a

general adherence to Carnelley's rule which relates higher molecular symmetry and increased melting points.^{11a-g,21}

Table 4: Melting point ranges (°C) of the **NxxCl**^{this work} and **Clxx** isomers^{11g}

NxxCl	NpxCl	NmxCl	NoxCl
NxpCl	139.0-140.0 (W)	168.3-172.9	138.0-140.0
NxmCl	164.0-166.0	139.2-141.6	90.8-92.1
NxoCl	132.7-134.7	80.0-81.9	110.1-111.5
Clxx	Clxp	Clxm	Clxo
Clpx	206.2-208.4	150.1-151.3	131.5-134.5
Clmx	185.4-187.2	112.4-113.9 (W)	95.0-105.0
Cloxx	167.9-169.9	134.5-137.8	134.4-138.0

Footnote: monohydrates are marked as (W)

The **Clxx** series provides an illustration of Carnelley's rule,²¹ (Table 4).^{11g} An empirical function based on substituent positions and the lattice electrostatic energy was introduced and allowed a multi-linear fit of the melting temperatures yielding a correlation coefficient with the experimental values larger than 95%. The correlation coefficient between the melting points of **Clxy** and **NxyCl** series is 51% (with **x**, **y** indicating *o*-/*m*-/*p*-substitution). Given the high degree of correlation, this model can be further refined in series of related benzamides and its possible predictive behaviour evaluated.

The **NxxCl** melting points have been measured in a similar fashion to previous measurements and also independently compared using a blind test. Of interest in Table 4 is that the average **NxxCl** melting point is 130°C and this is ~20°C less than the corresponding amide-bridged reversed **Clxx** isomers.^{11g} How does this difference in melting points arise for isomers that differ by so little (as amide-bridge reversed structures). The highest melting points are for **NmpCl** (170°C) and **NpmCl** (165°C) and the lowest are for **NmoCl** (68°C) and **NomCl** (91°C). The **NppCl** crystal as a monohydrate is kept separate and recorded for the sake of completion. The observed trends are what would be expected from molecular symmetry based on Carnelley's rule^{21b} and similar to our related series.^{11a-f}

As seen previously in the **Clxx** series^{11g} (average melting point of 148°C), the effect of chlorine substitution (compared to fluorine or methyl) is to bestow an average higher melting point of 17°C compared to **Fxx** (131°C), which is 15°C greater than **Mxx** (116°C) (in a trend as Br≈Cl>F>Me).²¹ Overall, the **Clxx**,^{11g} **Fxx**,^{11c} **Mxx**^{11d} series have higher average melting points than their corresponding amide bridge reversed **NxxCl** (130°C), **NxxF** (117°C)^{11a} and **NxxM** (113°C)^{11b} isomer grids. One partial answer must lie in presence of intramolecular N_{pyr}...H-N_{amide} hydrogen bonds in **NoxCl** structures. The equivalent but weaker Cl_{pyr}...H-N_{amide} hydrogen bonds are not formed in the **Cloxx** structures. The average *T_m* is 114°C for **NoxCl** and 123 K for **Cloxx**. Globally these subsets of structures with

intramolecular H-bonds have lower melting points than their **NmxCl** and **Clmx** counterparts which have the same molecular symmetry level (**Table 4**). The presence of the intramolecular H-bond results in weaker intermolecular interactions and electrostatic energy and, as a consequence, T_m is decreased, as discussed in the next paragraph. The rest of the answer must lie in intramolecular interactions and how the molecules pack in their respective crystal structures.

Melting points and electrostatic energy:

In order to relate the melting point temperatures T_m to energies, additional analyses were conducted to identify correlations. The **NppCl**•H₂O crystal structure which has a different chemical content was not included in the analysis.

The Gibbs free energy of a system depends on the temperature T , the enthalpy (ΔH) and entropy (ΔS) variations: $\Delta G = \Delta H - T\Delta S$. The free energy of melting vanishes at the temperature T_m and therefore $T_m = \Delta H_m / \Delta S_m$ (equation 1). According to equation (1), the melting point temperature is expected to increase when the enthalpy change ΔH_m is large. The crystal enthalpy is closely related to the computed lattice energy (the mechanical energy to separate the molecules to infinity keeping their crystalline electron distributions and their non relaxed geometry). The electrostatic component (E_{elec}) can be estimated directly using the multipolar atom model transferred from ELMAM2 electron density database.^{15a} The relationship between T_m and the lattice or electrostatic energy is investigated here.

In order to see some trends, **Table 5** shows the correlation between the melting points and several energetic and molecular symmetry descriptors of the non-hydrated **NxxCl** crystals. The quantities T_m and $-E_{elec}$ indeed show a small correlation ($R = 37\%$) in **Figure S01 (ESI)**. The three **NoxCl** compounds, with the intramolecular N-H...N hydrogen bond, have the weakest E_{elec} values. In our previous study of **Clxx** isomers,^{11g} the two properties showed a higher correlation of $R = 0.47$ and the compounds with strongest electrostatic lattice energy tended to have the highest melting points.

In the **Clxx** isomer series, it was observed that E_{HB} , the electrostatic energy between acceptor and donor atoms of the strongest hydrogen bond in the crystal, has an influence on the melting point. The T_m values were more correlated ($R = 0.63$) with the $-(E_{elec} - E_{HB})$ values than by considering $-E_{elec}$ exclusively. This suggested that contributions to ΔH_m are rather due to the weaker intermolecular interactions, as the strongest hydrogen bonds might subsist in the molten phases. The $(E_{elec} - E_{HB})$ quantity refers to the total electrostatic energy corrected by removing the strongest hydrogen bond contribution. In the **NxxCl** series as presented herein, this correlation $R = 0.44$ is more moderate but still stronger than $R(T_m, -E_{elec}) = 0.37$ (**Table 5**).

Table 5: Correlation coefficients between the experimental T_m values and computed properties. Correlations of T_m with T_{fit} melting points fitted by multiple regression are shown.

C_{XY} (Carnelley's rule)	0.76
$-E_{\text{elec}}$	0.37
$-(E_{\text{elec}} - E_{\text{HB}})$	0.44
$-E_{\text{tot}}$	0.46
$-(E_{\text{tot}} - E_{\text{HB}})$	0.64
$T_{\text{fit}}(E_{\text{elec}}, C_{XY})$	0.807
$T_{\text{fit}}(E_{\text{elec}} - E_{\text{HB}}, C_{XY})$	0.870
$T_{\text{fit}}(E_{\text{tot}}, C_{XY})$	0.887
$T_{\text{fit}}(E_{\text{tot}} - E_{\text{hb}}, C_{XY})$	0.873
$T_{\text{fit}}(E_{\text{tot}}, E_{\text{hb}}, C_{XY})$	0.888

Entropy is another key factor which plays a significant role in the melting point temperature in equation (1). Hence, according to the Carnelley rule,^{21a} a molecule with a higher rotational symmetry is expected to show a smaller increase in entropy ΔS_m when the crystal melts and, consequently an increased T_m temperature.

The *para*-substituted **NxxCl** compounds have a higher symmetry than the unsymmetrical *ortho*- and *meta*-substituted isomers. In **Figure 8**, the compounds with a *para*-substitution clearly show, on average, higher T_m values than the other isomers (105.9°C vs. 152.1°C). In order to model Carnelley's rule by accounting for its dependence on the substituent positions, the C_{XY} descriptor was defined for the **NxyCl** isomers: $C_{XY} = 1$ when one of the substitution positions is located as *para*, $C_{XY} = 0$ when there is no *para*-position. The resulting correlation between T_m and C_{XY} is 0.76.

A double linear regression to fit T_m against the Carnelley derived C_{XY} function and the lattice energy was also undertaken. This model accounts simultaneously for the enthalpic and the entropic contributions to the melting point T_m . The scatterplot of the T_m experimental and of the ones fitted from $(C_{XY}, E_{\text{elec}} - E_{\text{HB}})$ data shows a correlation of 0.87 (**Figure 9**), which is lower than the high value $R = 0.961$ observed for the **Clxx** benzamide series.^{11g} The same double regression using $(C_{XY}, E_{\text{elec}})$ properties leads to a fit of lower quality at $R = 0.81$ (**Figure S02 ESI**). As observed also for the **Clxx** series, when the E_{elec} and C_{XY} properties are combined, taking into account the E_{HB} energies of the strongest H-bond as a third variable does not improve significantly the linear fitting (Table 5).

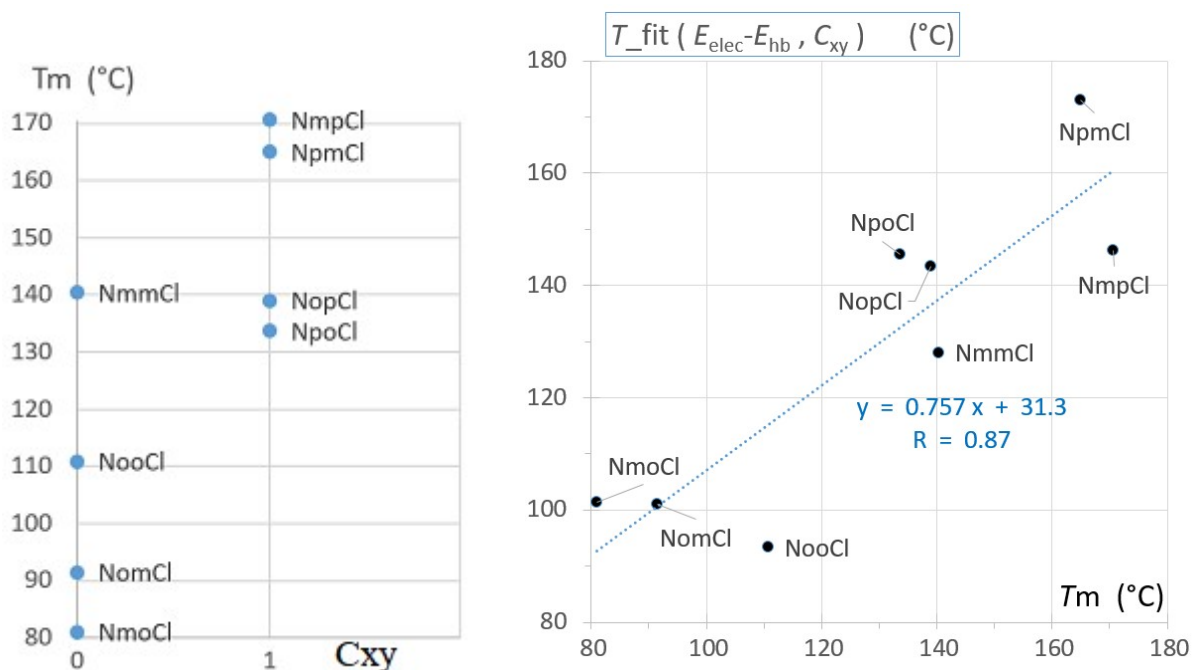


Figure 8 (left): Melting point in the isomers classified according to descriptor C_{XY} derived from Carnelley's rule: $C_{XY} = 1$ when x or y is p (*para*), $C_{XY} = 0$ (remainder).

Figure 9 (right): Double linear regression of the melting point T_m on the Carnelley molecule symmetry descriptor C_{XY} and the $E_{elec}-E_{HB}$ value, the electrostatic lattice energy diminished by the strongest hydrogen-bond electrostatic energy.

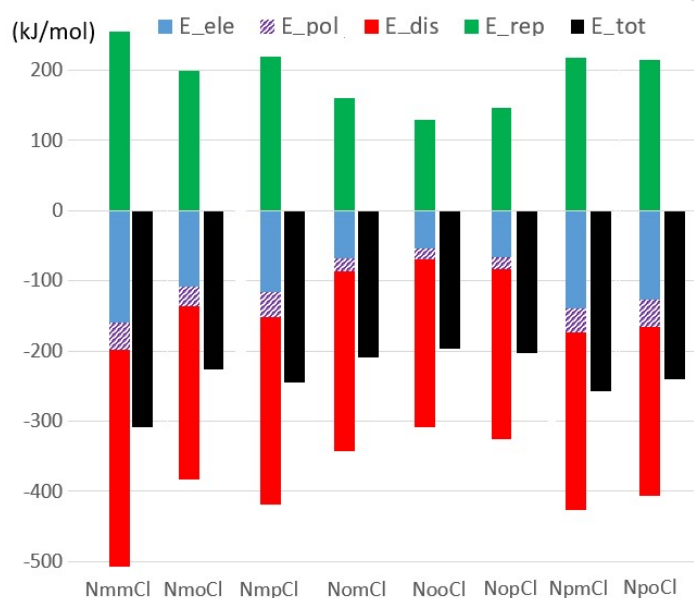


Figure 10. The components of the total lattice interaction energy of the $N_{xx}Cl$ molecules computed on a cluster of surrounding molecules with CrystalExplorer using CE-B3LYP. B3LYP/6-31G(d,p) electron densities.^{15d} In the summation of E_{tot} values, the electrostatic, polarization, dispersion and repulsion components were scaled (coefficients 1.057, 0.74, 0.871, 0.618) according to benchmarked energy models.^{15d}

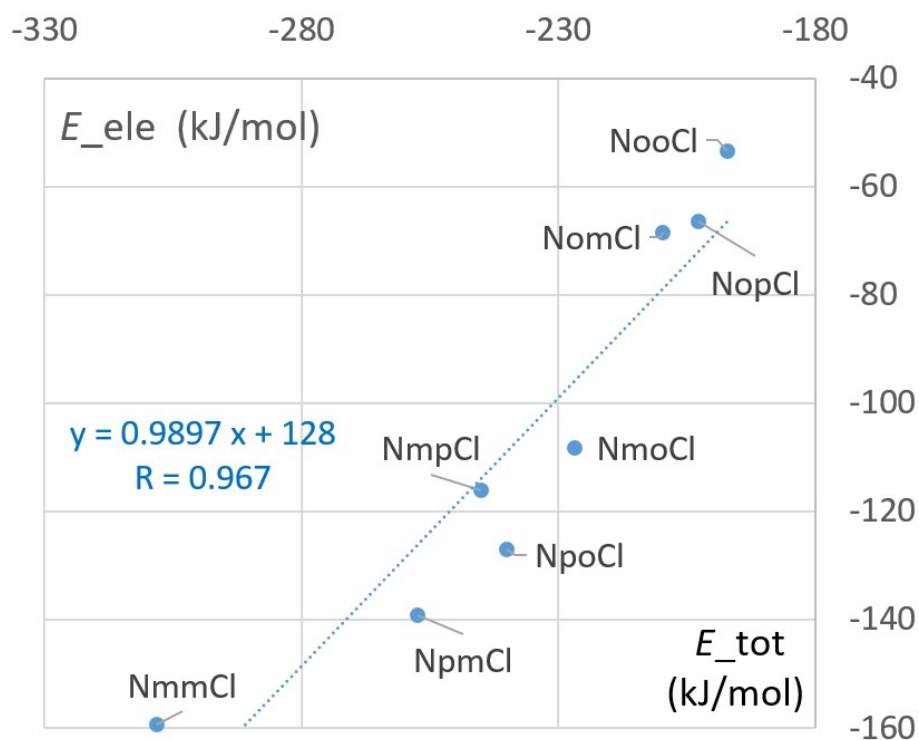


Figure 11. Scatterplot of total and electrostatic energy from CrystalExplorer (right).

The total lattice energy E_{tot} and its components have been computed with CrystalExplorer and are shown in **Figure 10**.^{15d} The electrostatic energy E_{ele} as derived from CrystalExplorer^{15d} and E_{elec} derived from ELMAM2^{15a} electron density database show an excellent correlation ($R = 0.967$) **Figure 11** but the former values are on average 25% higher than the ELMAM2 derived ones (**Figure S03**).^{15a} For the **NxxCl** series, the average electrostatic E_{ele} (from CrystalExplorer^{15d}) and dispersion E_{disp} values are -105 ± 38 and -257 ± 23 kJ/mol which shows that most of the lattice energy comes mostly from the dispersion component. This is related to the mostly hydrophobic character of the **NxxCl** molecules. The E_{disp} values show however low variations among the compounds and as a result the ranking of the E_{tot} values originates mostly from differences in E_{ele} values. This is confirmed by the scatterplot as depicted in **Figure S03** which shows globally increasing E_{tot} values as E_{ele} augments. The E_{tot} values can be approximated from the E_{ele} ones by a well-defined linear equation which has a slope close to unity and has an intercept value of approximately 128 kJ/mol. The T_m melting points are much more correlated with the total energy $-E_{tot}$ and $-(E_{tot} - E_{HB})$ (R reaching 0.64) compared to the equivalent values issued from electrostatic energy $-E_{elec}$ (**Table 5**, **Figure S04** and **Figure S05**). The double linear fit of T_m on E_{tot} and C_{xy} values yields a high $R = 0.887$ value (**Figure S06**; ESI).

Ab initio modelling studies and conformational analysis of the NxxCl isomer grid

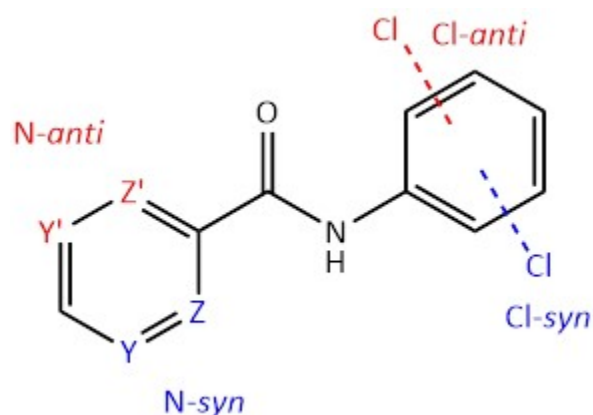
The molecular model geometries of the **NxxCl** isomers have been investigated and *ab initio* geometry optimisations undertaken using the DFT method (B3LYP/6-311++G(d,p)) with the Gaussian09 software.^{14a} The three resulting optimised torsion angles α , β and δ are tabulated in **Table 6**.

	α°	β°	δ°
NppCl	23.71	4.24	1.47
NpmCl	25.72	4.97	1.39
NpoCl	23.27	3.61	2.20
NmpCl	23.13	4.93	2.26
NmmCl	22.93	4.23	2.14
NmoCl	21.42	4.15	2.73
NopCl	0.00	0.00	0.00
NomCl	0.00	0.00	0.00
NooCl	0.00	0.00	0.00

Table 6: Torsion angles ($^\circ$) of the optimised **NxxCl** isomers^a

Footnote: ^a Angle C26–C21–C1=O1 (**N-ring**) refers to α ; C1–N1–C11–C12 (or **Cl-ring**) as β and the O1=C1–N1–C11 amide linkage as the δ angle. All geometries are based on B3LYP/6-311++G(d,p) optimisation in gas phase.¹⁴ The **NppCl** optimisation was undertaken on the molecule not the hydrate.

The optimised geometries of the nine **NxxCl** isomers (**Table 6**) closely resemble the geometries of their equivalent isomer grids *i.e.* **NxxF** and **NxxM**.^{11a,b} The **NoxCl** triad is completely planar with all torsion angles at 0.00° ; the planarity of the **NoxCl** triad is assumed by the intra-molecular N1–H1...N22 interaction.^{11a,b} On the other hand, the **NpxCl** and **NmxCl** triads have torsion angles more or less deviating from planarity. On average the α angle (*para*-/*meta*-pyridinyl ring, **N-ring**) is 23.36° ($\sigma = 1.27^\circ$), whereas the β torsion angle (chlorophenyl ring, **Cl-ring**) is 4.36° ($\sigma = 0.47^\circ$) and the δ torsion angle (amide linkage) is 2.03° ($\sigma = 0.47^\circ$).



Scheme 3:

Possible conformations of **NxxCl** as applied to the *ortho*-/*meta*-substitutions.

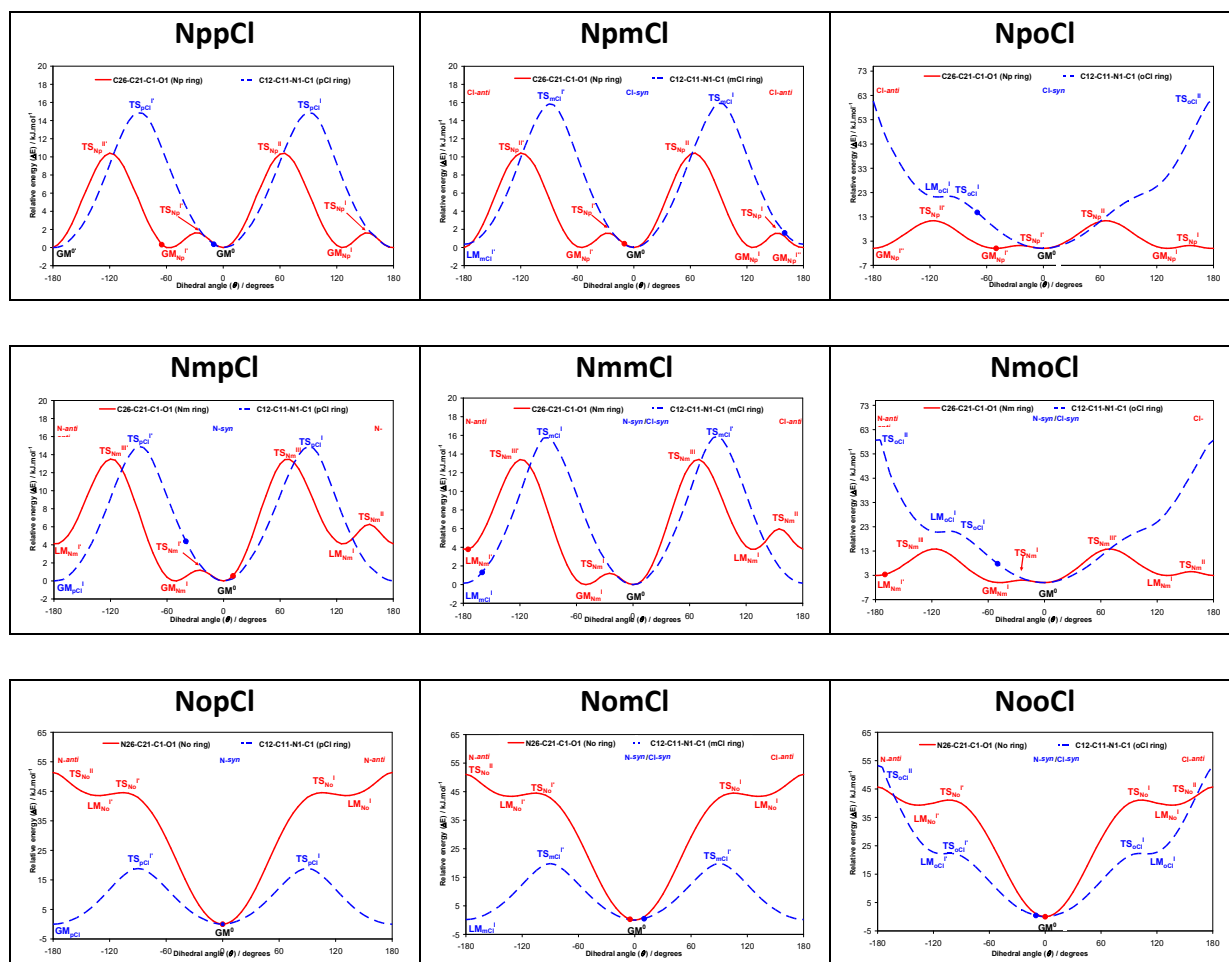


Figure 12: The Potential Energy Surface (PES) conformational analysis for the **NxxCl** isomers optimised in the gas phase: the equivalent solid-state angle is depicted by (●). Transition states (TS) and Global Minima (GM) are indicated and labelled. Enlarged high resolution figures are provided in the ESI.

The conformational analysis was undertaken using the B3LYP/6-311++G(d,p) method and basis set.^{14b,c} The PES conformational analysis diagrams (**Figure 12**) for the 3×3 **NxxCl** isomer grid reveal significant similarity with their related **NxxF** and **NxxM** series.^{11a,b} The N-ring and most of the Cl-ring PES profiles are similar with rotational barriers having comparable heights. However, the *ortho*-chlorophenyl ring (**oCl**-ring) shows a higher rotational barrier (53–60 kJ.mol⁻¹) as compared to the **oM**-ring (35 kJ.mol⁻¹) (**NxoM** triad)^{11b} and the **oF**-ring (50 kJ.mol⁻¹) (**NxoF**).^{11a} This is rationalised by factoring in the larger atomic radius of chlorine compared to fluorine or the methyl group. Other differences are for **NxoM/F/Cl** triads and the effect of the *ortho*-methyl group on the shape and height of the β torsion angle C1–N1–C11–C12(Me) compared to both F and Cl which can be explained on both steric (size) and electronic grounds (intramolecular hydrogen bonding involving F and Cl).

Conformational analysis suggests that the **N-syn** conformation (**Scheme 3**) of the N-ring is more stable (by 3.9 kJ.mol⁻¹) while the **mCl**-ring is just slightly stable (by 0.2 kJ.mol⁻¹) making the **Cl-anti** conformation a possibility (**Scheme 3**). As well as this the **N-anti** conformation is plausible but is less probable in the gas phase. The *ortho*- **oN**-ring and **oCl**-ring can be stable only when they are positioned in the *syn* conformation. In summary, all modelling predictions are consistent with previous studies on the **NxxF** and **NxxM** series.^{11a,b}

COMPARISONS OF CALCULATED MODELS WITH SOLID STATE STRUCTURES

Differences between the modelled and solid-state torsion angles (**N-ring** and **Cl-ring**) are marked with a dot (•) on each of the **NxxCl** PES curves (**Figure 12**). The solid-state conformations of the **NoxCl** triad match those of the modelled structures with little or no torsion angle deviation. The **NoxCl** molecules are planar both in the solid state and as models *e.g.* **NooCl** (**Figure 6**). Therefore, the N1-H1...N22 intra-molecular hydrogen bond and molecular planarity established in the optimized *ab initio* models is confirmed by the **NoxCl** solid-state structures. In **NomCl**, the **Cl-syn** conformation is preferred over **Cl-anti**; the **Cl-anti** would represent a disruption of the intramolecular hydrogen bonding while the **Cl-syn** assists in the formation of C23-H23...Cl13 intermolecular interactions.

In the **NpoCl** crystal structure, the **oCl**-ring deviates by -70° from the optimized model. This deviation is necessary to allow for the formation of amide...amide (N1-H1...O1=C1) intermolecular hydrogen bonds (**Figure 3**). The chlorine is positioned favourably, while the twisted **oCl**-ring allows for closer aggregation of **NpoCl** molecules and hydrogen bond formation. A similar rotation of the **oCl**-ring arises in **NmoCl** where a less pronounced change in the Cl-ring torsion angle assists in N1-H1...O1 hydrogen bond formation. In tandem, the N-ring adopts the **N-anti** conformation that is essential for the formation of both C14-H14...Cl12 interactions and other important contacts that assist in structure aggregation.

Both aromatic rings in **NmmCl** are in the **N-/Cl-anti** conformation and opposite to the modelled gas phase structure (**Figure 5**). The flipping of the N-ring into an **N-anti** conformation was already noted in **NmmF**^{11a} and **NmmM**^{11b} as it is critical for the formation of N1-H1...N23 hydrogen bonds and *zig-zag* chains. It is unclear why the Cl-rings in both of the **NmmCl** and **NpmCl** isomers are in a slightly less stable geometry by adopting the plausible **Cl-anti** conformation (**Figure 2**): the chlorine atoms do not engage in any close contacts or halogen bonding but rather are situated in a relatively interaction free position in the crystal structure. While the opposite **Cl-syn** conformation seems to be possible, there is no structural disorder observed (with a *syn-/anti-* swap), as noted for the analogous **NomF** isomer.^{11a} There are no conformational differences between the optimised and solid-state structures for the **NmpCl** isomer, while for the **NppCl** isomer, this formalism is not applicable on symmetry grounds with both *para*-ring substitutions.

CONTACTS ANALYSIS:^{15,20}

The intermolecular contact types on the Hirshfeld surface were analyzed in **NxxCl** using the MoProViewer software.^{15e} The proportions of the main contacts in the nine **NxxCl** crystal structures are shown in **Figure 13**. Contacts between two chemical types (X,Y) are over-represented when their proportion C_{xy} is larger than that obtained by probability products of the chemical contents S_x and S_y on the Hirshfeld surface.^{15e-g} Enrichment ratios are therefore obtained by dividing the actual proportion by the equiprobable reference value. The most enriched contacts are the strong N-H...N and N-H...O=C hydrogen bonding interactions with average enrichment ratios $\langle E \rangle$ larger than four (**Table 7**; ESI Table S5). The standard deviations of E_{HnO} and E_{HnN} are large as for many crystals one of these two E values is zero, as only one of such hydrogen bond types occurs. The three **NoxCl** isomers have an intramolecular N-H...N hydrogen bond (not counted in the Hirshfeld statistics) but are devoid of an intermolecular one (**Figure 6**). The **NmmCl**, **NmpCl** and **NpmCl** isomers display an intermolecular N-H...N hydrogen bond, whereas in both **NmoCl** and **NpoCl** isomers an N-H...O=C hydrogen bond is observed (**Figure 3**). As the **NxxCl** molecules have two strong hydrogen bond acceptors with a deficit of strong donors (only one N-H group is available), weak hydrogen bonds are also favored as $\text{pyridineN}\dots\text{H-C}$ and $\text{C=O}\dots\text{H-C}$. The enrichment ratios of E_{NHc} and E_{OHc} are -87% anti-correlated in the eight anhydrous crystal structure packings.

Among contacts between the C, H_c and Cl hydrophobic atoms, the weak Cl...H_c hydrogen bond are enriched. The C...C stacking contacts are also significantly enriched, as would be expected for heterocycles.^{15b} All of the nine crystal structures have Cl...H_c weak hydrogen bonds which are over-represented. This is easily understood as H_c is the chemical type which has the largest representation at 37% on the Hirshfeld surface and as organic halogen atoms are favored contact partners for H_c.^{20a,b}

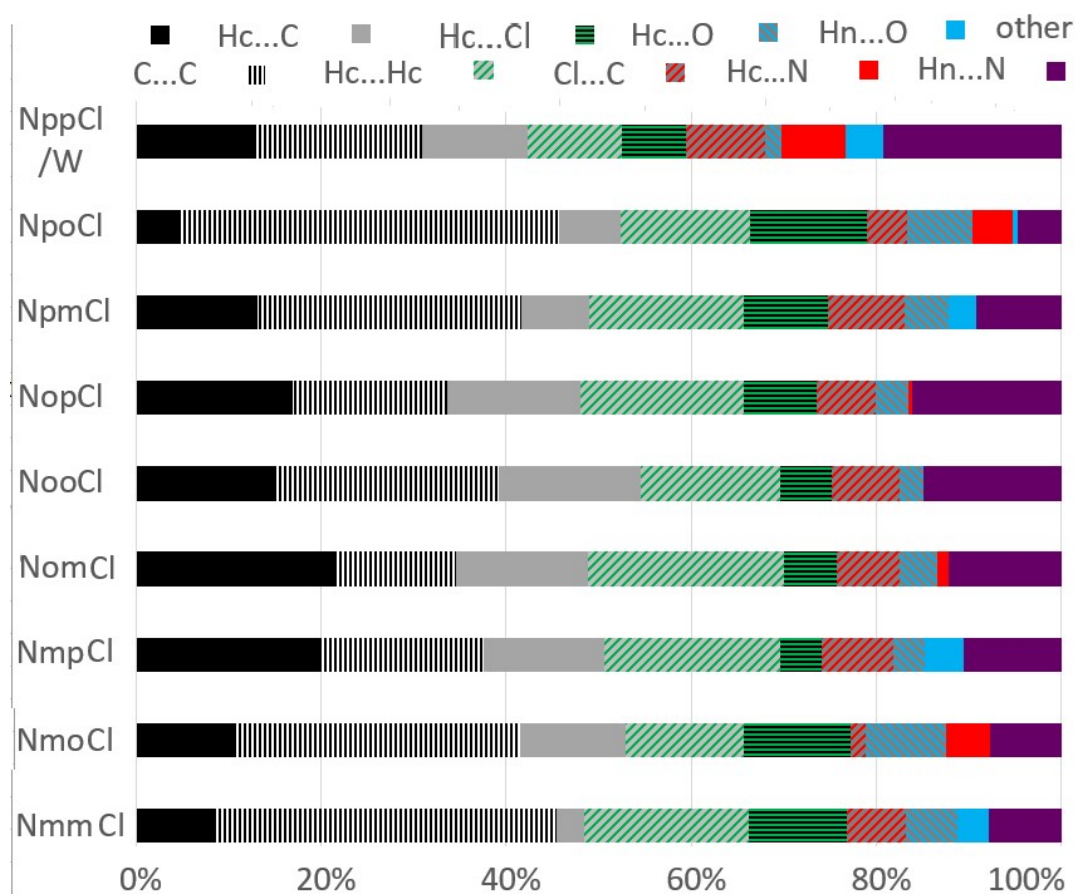


Figure 13: Contact proportions in the nine **NxxCl** isomer crystals.

Table 7: Average X...Y contacts enrichment ratios between the different chemical types in the 8 non-hydrated **NxxCl** crystal structures.

chem.	C	H _c	Cl	N	H _N	O
<surface> %	35.5	37.6	13.8	5.2	2.9	5.1
C	1.2(5)	1.0(4)	0.9(3)	1.0(6)	0.8(7)	0.6(3)
H _c		0.7(3)	1.6(3)	1.2(4)	0.7(4)	1.6(6)
Cl			0.6(7)	0.1(2)	0.0(1)	0.4(4)
N				0.9(11)	4.3(55)	0.1(2)
H _N					0.01(4)	4.5(69)
O						0.1(3)

Footnote: The sample standard deviations are given between parentheses (). The over-represented contacts are highlighted in **bold** characters. The second line shows the average chemical content on the Hirshfeld surface. The hydrophobic atoms C, H_c and Cl have been regrouped in the table. H_c and H_N refer to hydrogen atoms bound to carbon or nitrogen which are distinguished as they are chemically very different.

The **NxxCl** isomers have mostly hydrophobic atoms (C, H_c and Cl) at their Hirshfeld surface, with a proportion reaching 86%. The amount of purely hydrophobic contacts within these atoms is remarkably stable at $77 \pm 1.3\%$ for the eight non-hydrated **NxxCl** isomers and this corresponds to a global hydrophobic contacts enrichment of 1.03. In contrast, the

polar...polar contacts only represent 3% of the Hirshfeld surface but are globally over-represented with $E = 1.63$. The cross polar/hydrophobic contacts make a total of 20% of the surface and are moderately under-represented at $E = 0.84$ and are mainly due to weak C-H...O and C-H...N hydrogen bonds.

The **NpoCl** and **NmmCl** crystals are characterized by limited aromatic ring stacking as the two rings of the molecules have very different orientations (**Table 2**). Conversely, these two compounds have high amounts of weak C-H... π hydrogen bonds ($E_{\text{HCC}} = 1.56, 1.42$, respectively). In **NpoCl**, the two aromatic rings are nearly perpendicular (with $C_6/C_5N = 83.24(7)^\circ$ in **Table 2**) and this crystal packing consequently exhibits extensive C-H... π interactions.^{5c} On the other hand, **NmpCl** and **NomCl** crystals show extensive aromatic ring stacking and the two aromatic rings of each molecule are effectively parallel.^{5f} In the **NomCl** packing, all the molecules are close to planarity and are essentially parallel [$C_6/C_5N = 1.07(6)^\circ$]; while in **NmpCl** the aromatic rings have an orientation of $C_6/C_5N = 7.65(14)^\circ$. Therefore, in summary, the C...C and C...Hc enrichment values are -96.8% anti-correlated in the eight anhydrous **NxxCl** structures. Similarly, for contacts proportions C_{xy} , the anti-correlation of enrichments reaches -90.4%.

In broad terms, chlorine...chlorine contacts are generally avoided (with $\langle E \rangle = 0.6$) but with the exception of **NmpCl** and **NooCl**. In these two crystal structures, the Cl...Cl contacts do not correspond to halogen bonds (where the σ -hole faces the electronegative crown) but are merely at the van der Waals contact level and result from the translation of molecules along a short unit cell axis.

In order to find some hints why the **NxxF** series^{11a} shows poor isomorphism with the **NxxCl** series, the contact enrichments of F and Cl atoms were compared in **Table S6** (ESI). One major difference is that the **NxxF** series showed an average enrichment of only 1.3 for the F...Hc weak hydrogen bonds when compared to 1.6 for the Cl...Hc intermolecular interactions in **NxxCl**. Of note is that Feng and co-workers have shown by rotational spectroscopy, that in a competition between weak H-bonds in the $\text{CH}_2\text{FCl}\cdot\text{H}_2\text{C}=\text{O}$ adduct, the C-H...Cl intermolecular interaction is preferred to C-H...F.²²

From a charge density topology point of view, the strengths of H...Cl hydrogen bonds appear to be also more important than that of the H...F type.²³ Indeed, a starting degree of covalence appears at longer distances for Cl than for F.^{23b} Accordingly, for a given internuclear distance H...halogen (halogen = F, Cl), the electron density at the bond critical point of H...Cl is larger than at that of H...F, because the penetration of electron-shells is more important in the case of Cl.^{23a} Hence, due to the higher electronegativity of F compared to Cl, the H...F interaction tends to be more closed-shell in nature and a significant shared-shell character can be only present at very short H...F geometries. In addition, within the Natural Bond Orbital theory (NBO),²⁴ it has been established that charge

transfer from the acceptor (halogen) towards the X-H σ^* molecular-orbital can be considered as the signature of the X-H...(halogen) hydrogen bond strength. Again, due to the larger electronegativity of F, charge transfer in hydrogen bonds will be less important with F than with Cl, leading to weaker interactions with the former acceptor. The interactions propensity of fluorine is different from those of chlorine and bromine, and this might explain the lower isomorphism of **NxxF** with the **NxxCl** series, compared to **NxxBr**.

In conclusion, the **NxxCl** crystal structures fulfill the following contacts in order of priority: (i) one strong intra or inter-molecular hydrogen bond, involving N-H and N_{pyridine} or O=C, (ii) the remaining hydrogen acceptor atom interacts with H_C atoms, (iii) weak C-Cl...H_C hydrogen bonds are always formed, (iv) hydrophobic interactions between the H_C and C atoms represent, on average, 50%±2% of the contact surface and (v) aromatic ring stacking is favored when the two rings and their symmetry related partners have similar orientations, while weak C-H... π hydrogen bonding interactions occur mostly when the aromatic ring orientations differ significantly.

In our previous studies with **Clxx**^{11g}, we have noted the paucity of halogen bonding and notably Cl...Cl contacts in these amide-bridge reversed isomers. This behavior is not too dissimilar to that observed for **NxxCl**. In related research, we have considered the competition between the F, O=C, N-H and aromatic rings in terms of influencing interactions and aggregation.^{6d} We have also speculated on the number of halogen atoms and type of halogen atom needed to tip the interactions from hydrogen bonding towards halogen bonding of the type C-Cl...O=C, C-Cl...N_{pyridine} and C-Cl...Cl-C. Indeed, research studies on the competition between interactions in crystal structure formation has been pursued with much interest recently and especially in co-crystal formation.²⁵

In research concerning the competition between hydrogen-bonding and halogen-bonding interactions in the crystal structures of pentachlorophenol (C₆Cl₅OH) and pentabromophenol (C₆Br₅OH), it has been pointed out that (C)O-H...O(H)-C is stronger than solitary C-Cl...Cl-C and C-Br...Br-C interactions, as observed from the topological properties of $\rho(\mathbf{r})$ at the corresponding bond critical points (H...O > Br...Br > Cl...Cl).²⁶ Similar conclusions were also raised with the electrophilic-nucleophilic interactions between the corresponding local charge concentration (CC) and charge depletion (CD) sites in the valence shell of atoms involved in the intermolecular interactions (H...O > Br...Br > Cl...Cl), here characterized by the topology of $L(\mathbf{r}) = -\nabla^2\rho(\mathbf{r})$. In both crystal structures, neither O-H...Cl-C nor O-H...Br-C intermolecular hydrogen bonds are observed, indicating that O is a better acceptor in O-H...O(H)-C hydrogen bonds than Cl and Br in the former. On the other hand, halogen-bonding of the C-Cl...O(H)-C and C-Br...O(H)-C type is neither observed, because involving O as acceptor in (C)O-H...O(H)-C hydrogen-bonds leads to stronger interactions. Consequently, if halogen bonding of the type C-Hal...O=C, C-Hal...N_{pyridine} or C-Hal...Hal-C should compete with H...O=C, H...N_{pyridine} and H...Hal-C hydrogen bonds, the best candidates should be found

with the heavier halogens (Hal = Br, I), otherwise the number of acceptors should be larger to permit Hal-atoms to take place in donors once the best donors have been used up.

SUMMARY AND CONCLUSIONS

The 3×3 isomer grid of **NxxCl** [*N*-Chlorophenyl(pyridine)carboxamides] structures displays correlations with their **NxxX** (X = F, Br or M = Me) analogues. This is readily demonstrated with five isomorphous relationships between pairs of structures involving the **NxxCl** and **NxxBr** counterparts.^{11e,18a,c} The behaviour mimics the amide-bridge reversed **Clxx** series^{11g} in its relationships with both methyl and bromo-substituted derivatives but not with the fluorine analogues. As such there is a transition along the Me→F→Cl→Br series of structures where the increasing influence of the halogen atom is noted, its effect on the structure and the increased structural overlap (isomorphous behaviour) between the Cl and Br derivatives as noted here in **NxxCl** and for **NxxBr**.^{11e}

N-H...N interactions dominate in comparison to N-H...O=C in the **NxxCl** series. This has been noted over several structural series¹¹ between molecules where there is direct competition between the O=C and N_{pyridine} as acceptors of the N-H amide hydrogen bond donor group. The remaining O or N acceptor atom usually interacts with aromatic C-H groups. Weak C-H...Cl interactions are often present in the **NxxCl** structures but not in any predictable way. The planar **NooCl** structure is peculiar with its intra-molecular Cl...Hn...N_{pyridine} synergistic combination. Aromatic ring interactions arise especially where symmetry favours stacking and C-H...π interactions occur often where the aromatic plane orientations differ significantly. In models, the optimised geometries of the **NxxCl** isomers mostly resemble the geometries of related isomer grids *i.e.* **NxxF** and **NxxM**.^{11a,b} They also mostly correspond with their crystal structures and differences arise if there is a favourable interaction in the crystal structure that necessitates a change in **NxxCl** geometry. In doing so, the divergence between the models and solid-state geometry is more than compensated for in crystal packing forces and resulting favourable lattice energy. At the solid/liquid boundary the melting point of a member of the **NxxCl** series follows Carnelley's rule on molecular symmetry but with distinct differences (typically lower average melting points) than noted for their **Clxx** analogues.^{11g}

The 18-member series of **Brxx/NxxBr** structures is in preparation for publication with additional contact analysis and for comparisons with **NxxX** (X = F,^{11a} Cl,^{this work} or M = Me^{11b}) analogues together with their corresponding amide-bridge reversed isomers (**Mxx**,^{11d} **Fxx**,^{11c} **Clxx**^{11g}). The role and influence of the heavier halogen in the crystal structures will be assessed. Investigations on the physicochemical properties and trends of series of isomers of 72+ molecules (including polymorphs) will be available for future computational analysis.

ACKNOWLEDGEMENTS

This research was initially funded by the Programme for Research in Third Level Institutions (PRTL) Cycle 4 (Ireland) and co-funded through the European Regional Development Fund (ERDF), part of the European Union Structural Funds Programme (ESF). JFG thanks the School of Chemical Sciences, Dublin City University for grants in aid of chemical and crystallographic research. The Irish Centre for High End Computing (ICHEC) is thanked for support and assistance with the computational calculations (<http://www.ichec.ie>). PM thanks the T³ (PRTL-IV) program for a studentship. We also thank Ms. Karoline Benedet (UNESC, Santa Catarina, Brasil) for technical assistance on the melting point measurements. JFG together with EA, EE, BG and CJ thank the Université de Lorraine and Region Lorraine for a “Chercheur d’Avenir” grant.

SUPPLEMENTARY INFORMATION

Crystallographic data for the nine **NxxCl** crystal structures have been deposited with the Cambridge Crystallographic Data Centre, CCDC no. 2074347 to 2074355. CIF data may be downloaded from the CCDC website <https://summary.ccdc.cam.ac.uk/structure-summary-form> or obtained free of charge from The Director, CCDC, 12 Union road, Cambridge, CB2 1EZ, U.K. (fax: +44-1223-336033; e-mail: deposit@ccdc.cam.ac.uk). The data are available as CIF files from the corresponding author Dr. John F. Gallagher.

REFERENCES

1. (a) G. W. Gribble, *Chem. Soc. Rev.* (1999), **28**, 335–346. (b) G. W. Gribble, *Chemosphere*, (2003), **52**, 289–297. (c) G. W. Gribble, *Environmental Chemistry*, (2015), **12**, 395–405. (d) L. J. Jin and B. J. Chen, *Progress in Chemistry*, (2017), **29**, 1093–1114.
2. (a) K. Müller, C. Faeh and F. Diederich, *Science*, (2007), **317**, 1881–1886. (b) J. Wang, M. Sánchez-Roselló, J. L. Aceña, C. del Pozo, A. E. Sorochinsky, S. Fustero, V. A. Soloshonok and H. Liu, *Chem. Rev.* (2014), **114**, 2432–2506. (c) B. Klencsar, C. Sanchez, L. Balcaen, J. Todoli, F. Lynen, F. A. F. Vanhaecke, *J. Pharm. and Biomed. Analysis*, (2018), **153**, 133–144. (d) G. Berger, J. Soubhye, R. Wintjens, K. Robeyns and F. Meyer, *Acta Crystallogr.* (2018), **B74**, 618–627.
3. (a) R. E. Banks, B. E. Smart and J. C. Tatlow. Eds., *Organofluorine chemistry: Principles and Commercial Applications*, (1994), **11**, Springer Science. (b) C. D. Murphy, *J. Applied Microbiology*, (2003), **94**, 539–548. (c) P. Jeschke, *Pest Manage. Sci.* (2010), **66**, 10–27. (d) P. Jeschke, *Pest Manage. Sci.* (2017), **73**, 1053–1066. (e) J. Latham, E. Brandenburger, S. A. Shepherd, B. R. K. Menon and J. Micklefield, *Chem. Rev.* (2018), **118**, 232–269. (f) P. Mocilac and J. F. Gallagher, *CrystEngComm*, (2019), **21**, 4048–4062.
4. (a) P. Metrangolo and G. Resnati, Eds., *Halogen Bonding: Fundamentals and Applications; Structure and Bonding*, Springer, Berlin, (2008), **126**. (b) K. Raatikainen and K. Rissanen, *Chem. Sci.* (2012), **3**, 1235–1239. (c) G. R. Desiraju, P. S. Ho, L. Kloo, A. C. Legon, R. Marquardt, P. Metrangolo, P. Politzer, G. Resnati and K. Rissanen, *Pure Appl. Chem.* (2013), **85**, 1711–1713. (d) A. Mukherjee and G. R. Desiraju, *IUCrJ*, (2014), **1**, 49–60. (e) O. Makhothkina, J. Lieffrig, O. Jeannin, M. Fourmigué, E. Aubert and E. Espinosa, *Cryst.*

- Growth Des.* (2015), **15**, 3464–3473. (f) A. Bauza, T. J. Mooibroek and A. Frontera, *ChemPhysChem*, (2015), **16**, 2496–2517. (g) G. Cavallo, P. Metrangolo, R. Milani, T. Pilati, A. Priimagi, G. Resnati, G. A. F. Terraneo, *Chem. Rev.* (2016), **116**, 2476–2601. (h) M. H. Kolar and P. Hobza, *Chem. Rev.* (2016), **116**, 5155–5187. (i) J. C. Christopherson, F. Topic, C. J. Barrett and T. Frisic, *Cryst. Growth Des.* (2018), **18**, 1245–1259. (j) R. Tepper and U. S. Schubert, *Angew. Chem. (Int. Ed. Engl.)* (2018), **57**, 6004–6016. (k) A. M. S. Riel, D. A. Decato, J. Sun, C. J. Massena, M. J. Jessop and O. B. Berryman, *Chem. Sci.* (2018), **9**, 5828–5836. (l) R. Shukla, N. Claiser, M. Souhassou, C. Lecomte, S. J. Balkrishna, S. Kumara and D. Chopra, *IUCrJ* (2018), **5**, 647–653.
5. (a) G. R. Desiraju and T. Steiner, *The weak hydrogen bond in structural chemistry and biology*, (2001), Oxford University Press, UK. (b) A. Domenicano and I Hargittai, *Strength from Weakness: Structural Consequences of Weak Interactions in Molecules, Supramolecules and Crystals*, (2002), **68**, NATO Science series II, Springer Netherlands. (c) M. Nishio, *CrystEngComm*, (2004), **6**, 130–158. (d) I. Dance and M. Scudder, *CrystEngComm*, (2009), **11**, 2233–2247. (e) S. Alvarez, *Dalton Trans.* (2013), **42**, 8617–8636. (f) C. R. Martinez and B. L. Iverson, *Chem. Sci.* (2012), **3**, 2191–2201.
 6. (a) D. Chopra and T. N. Guru Row, *CrystEngComm* (2008), **10**, 54–67. (b) K. Donnelly, J. F. Gallagher and A. J. Lough, *Acta Crystallogr.* (2008), **C64**, o335–o340. (c) S. N. Nayak, M. K. Reddy, D. Chopra and T. N. Guru Row, *CrystEngComm*, (2012), **14**, 200–210. (d) P. Mocilac, I. A. Osman and J.F. Gallagher, *CrystEngComm*, (2016), **18**, 5764–5776.
 7. (a) G. Luthe, D. C. Swenson and L. W. Robertson, *Acta Crystallogr.* (2007), **B63**, 319–327. (b) J. Klösener, D. C. Swenson, L. W. Robertson and G. Luthe, *Acta Crystallogr.* (2008), **B64**, 108–119. (c) D. Choquesillo-Lazarte, V. Nemek and D. Cincic, *CrystEngComm*. (2017), **19**, 5293–5299.
 8. (a) C. C. Council, *Glob. Insights*, (2006), 1–13. (b) W. Chen, R. A. Mook Jr., R. T. Premont and J. Wang, *Cell Signal*, (2018), **41**, 89–96. (c) W. W. Gao, L. Gopala, R. R. Y. Bheemanaboina, G.-B. Zhang, S. Li and C. H. Zhou, *Eur. J. Med. Chem.* (2018), **146**, 15–37. (d) W. W. Wang, Z. Dong, J. Zhang, X. Z. Zhou, X. J. Wei, F. S. Cheng, B. Li and J. Y. Zhang, *Frontiers in Vet. Sci.* (2019), **6**, 294. (e) W. Y. Fang, L. Ravindar, K. P. Rakesh, H. M. Manukumar, C. S. Shantharam, N. S. Alharbi and H. L. Qin, *Eur. J. Med. Chem.* (2019), **173**, 117–153.
 9. (a) K. Naumann, *Pest. Manag. Sci.* (2000), **56**, 3–21. (b) T Kosjek and E. Heath, *Halogenated Heterocycles*, (2012), **27**, 219–246. (c) R. Jayaraj, P. Megha and P. Sreedev, *Interdiscip. Toxicol.* (2016), **9**, 90–100. (d) M. Rani, U Shankar and V. Jassal, *J. Environ. Manage.* (2017), **190**, 208–222.
 10. C. R. Groom, I. J. Bruno, M. P. Lightfoot, S. C. Ward, *Acta Crystallogr.* (2016), **B72**, 171–179.
 11. (a) P. Mocilac, A. J. Lough, J. F. Gallagher, *CrystEngComm*, (2011), **13**, 1899–1909. (b) P. Mocilac, J. F. Gallagher, *CrystEngComm*, (2011), **13**, 5354–5366. (c) P. Mocilac, K. Donnelly, J. F. Gallagher, *Acta Crystallogr.* (2012), **B68**, 189–203. (d) P. Mocilac, M. Tallon, A. J. Lough, J. F. Gallagher, *CrystEngComm*, (2010), **12**, 3080–3090. (e) Niall Hehir, Dublin

- City University, Ireland, PhD thesis, (2017). (f) J. F. Gallagher, S. Alley, M. Brosnan and A. J. Lough, *Acta Crystallogr.* **B66**, 196–205. (g) J. F. Gallagher, M. Farrell, N. Hehir, P. Mocilac, E. Aubert, E. Espinosa, B. Guillot and C. Jelsch, *Cryst. Growth Des.* (2019), **19**, 6141–6158.
12. (a) P. Mocilac and J. F. Gallagher, *Cryst. Growth Des.* (2013), **13**, 5295–5304. (b) J. F. Gallagher, S. Alley and A. J. Lough, *Inorg. Chim. Acta*, (2016), **444**, 113–125. (c) P. Mocilac and J. F. Gallagher, *Structural Chemistry*, (2017), **28**, 697–708.
13. (a) G. M. Sheldrick, *Acta Crystallogr.* (2015), **C71**, 3–8. (b) Oxford Diffraction, *CrysAlis CCD and CrysAlis RED*, (2010), Yarnton, Oxfordshire, U.K. (c) R. C. Clark, J. S. Reid, *Comput. Phys. Commun.* (1998), **111**, 243–257. (d) A. L. Spek, *Acta Crystallogr.* (2009), **D65**, 148–155. (e) C. F. Macrae, P. R. Edgington, P. McCabe, E. Pidcock, G. P. Shields, R. Taylor, M. Towler, J. van De Streek, *J. Appl. Cryst.* (2006), **39**, 453–457.
- 14 (a) M. J. Frisch *et al.*, *Gaussian 09 Revision B.01*, (2010), Gaussian Inc. Wallingford CT USA. (b) A. D. Becke, *J. Chem. Phys.* (1993), **98**, 5648–5652. (c) R. Krishnan, J. S. Binkley, R. Seeger and J. A. Pople, *J. Chem. Phys.* (1980), **72**, 650–654.
15. (a) S. Domagała, B. Fournier, D. Liebschner, B. Guillot and C. Jelsch, *Acta Crystallogr.* (2012), **A68**, 337–351. (b) C. Jelsch, B. Guillot, A. Lagoutte and C. Lecomte, *J. Appl. Cryst.* (2005), **38**, 38–54. (c) F. H. Allen and I. J. Bruno, *Acta Crystallogr.* (2010), **B66**, 380–386. (d) C.F. Mackenzie, P. R. Spackman, D. Jayatilaka and M. A. Spackman, *IUCrJ*, **4**, 575–587. (e) B. Guillot, E. Espinosa, L. Huder and C. Jelsch, *Acta Crystallogr.* (2014), **A70**, C279. (f) N. K. Hansen and P. Coppens, *Acta Crystallogr.* (1978), **A34**, 909–921. (g) A. Volkov, T. Koritsanszky and P. Coppens, *Chem. Phys. Lett.* (2004), **391**, 170–175.
16. (a) P. Mocilac, J. F. Gallagher and C. J. Jelsch, *Croat. Chim. Acta*, (2018), **91**, 281–288.
- 17 (a) T. N. Guru Row, *Coord. Chem. Rev.*, (1999), **183**, 81–100. (b) G. Tuchalski, F. Emmerling, K. Groger, A. Hansicke, T. Nagel and G. Reck, *J. Mol. Struct.* (2006), **800**, 28–44. (c) A. Abad, C. Agullo, A. C. Cunat, C. Vilanova, M. C. R. de Arellano, *Cryst. Growth Des.* (2006), **6**, 46–57. (d) S. Cuffini, C. Glidewell, J. N. Low, A. G. de Oliveira, M. V. N. de Souza, T. R. A. Vasconcelos, S. M. S. V. Wardell and J. L. Wardell, *Acta Crystallogr.* (2006). **B62**, 651–665. (e) T. Gelbrich, M. B. Hursthouse and T. L. Threlfall, *Acta Crystallogr.* (2007), **B63**, 621–632. (f) S. M. S. V. Wardell, M. V. N. de Souza, T. R. A. Vasconcelos, M. L. Ferreira, J. L. Wardell, J. N. Low and C. Glidewell, *Acta Crystallogr.* (2008). **B64**, 84–100. (g) F. Dumitru, Y.-M. Legrand, M. Barboiu and A. van der Lee, *Acta Crystallogr.* (2013), **B69**, 43–54. (h) P. Bombicz, *Crystallogr. Rev.*, (2017), **23**, 118–151.
- 18 (a) R. G. D. Taylor, B. R. Yeo, A. J. Hallett, B. M. Kariuki and S. J. A. Pope, *CrystEngComm.* (2014), **16**, 4641–4652. (b) Q. Zhang, S.-P. Zhang and S.-C. Shao, *Acta Crystallogr.* (2006), **62**, o4695–o4696. (c) D. Percival, J. D. A. Storey and W. T. A. Harrison, *Acta Crystallogr.* (2007). **E63**, o1851–o1852. (d) Y.-T. Park, C.-H. Jung, K.-W. Kim and H. S. Kim, *J. Org. Chem.* (1999). **64**, 8546–8556.
- 19 (a) W. H. Ojala, J. M. Smieja, J. M. Spude, T. M. Arola, M. K.; Kuspa, N. Herrera and C. R. Ojala, *Acta Crystallogr.* (2007), **B63**, 485–496. (b) K. J. Kassekert, T. J. Smith, J. M.

- Fermanich, K. M. Lystad, T. A. Gregoire, C. R. Ojala and W. H. Ojala, *Cryst. Growth Des.* (2019), **19**, 5896–5906.
- 20 (a) C. Jelsch, C. Ejsmont and L. Huder, *IUCrJ*, (2014), **1**, 119–128. (b) C. Jelsch, S. Soudani and C. Ben Nasr, *IUCrJ*, (2015), **2**, 327–340.
- 21 (a) R. Abramowitz and S. H. Yalkowsky, *Pharm. Res.* (1990), **7**, 942–947. (b) R. J. C. Brown and R. F. C. Brown, *J. Chem. Ed.* (2000), **77**, 724–731. (c) P. Vishweshwar, A. Nangia and V. M. Lynch, *Cryst. Growth Des.* (2003), **3**, 783–790. (d) Y. L. Slovokhotov, I. S. Neretin and J. A. K. Howard, *New J. Chem.* (2004), **28**, 967–979. (e) M. Podsiadlo, M. Bujak and A. Katrusiak, *CrystEngComm*. (2012), **14**, 4496–4450. (f) K. F. Dziubek and A. Katrusiak, *Acta Crystallogr.* (2014), **B70**, 492–497. (g) S. H. Yalkowsky, *J. Pharm. Sci.* (2014), **103**, 2629–2634. (h) R. K. Gamidi and A. Rasmuson, *Cryst. Growth Des.* (2017), **17**, 175–182.
- 22 G. Feng, Q. Gou, L. Evangelisti, M. Vallejo-López, A. Lesarri, E. J. Cocinero and W. Caminati, *Phys. Chem. Chem. Phys.*, (2014), **16**, 12261–12265.
- 23 (a) I. Mata, I. Alkorta, E. Molins and E. Espinosa, *Chem.–Eur. J.*, (2010), **16**, 2442–2452. (b) E. Espinosa, I. Alkorta, J. Elguero and E. Molins, *J. Chem. Phys.*, (2002), **117**, 5529–5542.
- 24 F. Wheinhold and C. R. Landis, *Valency and Bonding – A Natural Bond Orbital Donor-Acceptor Perspective*, (2005), Cambridge University Press, Cambridge, UK.
- 25 (a) E. Corradi, S. V. Meille, M. T. Messina, P. Metrangolo and G. Resnati, *Angew. Chem. Int. Ed.* (2000), **39**, 1782–1786. (b) C. B. Aakeröy, M. Fasulo, N. Schultheiss, J. Desper and C. Moore, *J. Am. Chem. Soc.* (2007), **129**, 13772–13773. (c) X. An, H. Zhuo, Y. Wang and Q. Li, *J. Mol. Model.*, (2013), **19**, 4529–4535. (d) K. Kowalska, D. Trzybiński and A. Sikorski, *CrystEngComm* (2015), **17**, 7199–7212. (e) C. C. Robertson, J. S. Wright, E. J. Carrington, R. N. Perutz, C. A. Hunter and L. Brammer, *Chem. Sci.* (2017), **8**, 5392–5398.
- 26 M. E. Brezgunova, E. Aubert, S. Dahaoui, P. Fertey, S. Lebègue, C. Jelsch, J. G. Angyan and E. Espinosa, *Cryst. Growth & Des.*, (2012), **12**, 5373–5386.